Automatica 141 (2022) 110296

Contents lists available at ScienceDirect

Automatica

journal homepage: www.elsevier.com/locate/automatica

Optimal and two-step adaptive quantum detector tomography☆

Shuixin Xiao [a,b], Yuanlong Wang [c,d], Daoyi Dong [b,*], Jun Zhang [a,*]

[a] University of Michigan – Shanghai Jiao Tong University Joint Institute, Shanghai Jiao Tong University, Shanghai 200240, China
[b] School of Engineering and Information Technology, University of New South Wales, Canberra ACT 2600, Australia
[c] Centre for Quantum Computation and Communication Technology (Australian Research Council), Centre for Quantum Dynamics, Griffith University, Brisbane, Queensland 4111, Australia
[d] Key Laboratory of Systems and Control, Academy of Mathematics and Systems Science, Chinese Academy of Sciences, Beijing 100190, China

ARTICLE INFO

Article history:
Received 16 June 2021
Received in revised form 14 December 2021
Accepted 14 January 2022
Available online 20 April 2022

Keywords:
Quantum detector tomography
Quantum system identification
Adaptive estimation
Quantum systems

ABSTRACT

Quantum detector tomography is a fundamental technique for calibrating quantum devices and performing quantum engineering tasks. In this paper, we design optimal probe states for detector estimation based on the minimum upper bound of the mean squared error (UMSE) and the maximum robustness. We establish the minimum UMSE and the minimum condition number for quantum detectors and provide concrete examples that can achieve optimal detector tomography. In order to enhance the estimation precision, we also propose a two-step adaptive detector tomography algorithm to optimize the probe states adaptively based on a modified fidelity index. We present a sufficient condition on when the estimation error of our two-step strategy scales inversely proportional to the number of state copies. Moreover, the superposition of coherent states is used as probe states for quantum detector tomography and the estimation error is analyzed. Numerical results demonstrate the effectiveness of both the proposed optimal and adaptive quantum detector tomography methods.

1. Introduction

In the past decades, we have witnessed significant progress in a variety of fields of quantum science and technology, including quantum computation (DiVincenzo, 1995), quantum communication (Nielsen & Chuang, 2010) and quantum sensing (Degen, Reinhard, & Cappellaro, 2017). In these applications, a fundamental task is to develop efficient estimation and identification methods to acquire information of quantum states, system parameters and quantum detectors. There are three typical classes of quantum estimation and identification tasks: (i) quantum state tomography (QST) which aims to estimate unknown states (Hou et al., 2016; Mu, Qi, Petersen, & Shi, 2020; Qi et al., 2013); (ii) quantum process tomography which targets in identifying parameters of evolution operators (Fiurášek & Hradil, 2001; Wang et al., 2019; Xiao, Xue, Dong and Zhang, 2021; Yu, Dong, Wang, & Petersen, 2020; Yu, Wang, Dong, & Petersen, 2021) (e.g., the system Hamiltonian (Sone & Cappellaro, 2017a, 2017b; Wang et al., 2018, 2020; Zhang & Sarovar, 2014, 2015)); and (iii) quantum detector tomography (QDT) which aims to identify and calibrate quantum measurement devices. In this paper, we focus on QDT and aim to present optimal and adaptive strategies for enhancing the efficiency and precision of QDT.

For general QDT protocols, the first solution was proposed in Fiurášek (2001) using maximum likelihood estimation (MLE). Subsequent works divide quantum detectors into phase-insensitive detectors and phase-sensitive detectors. Phase-insensitive detectors only have diagonal elements in the photon number basis, and therefore are relatively straightforward to be characterized using linear regression (Grandi, Zavatta, Bellini, & Paris, 2017), function fitting (Renema et al., 2012), or convex optimization (Feito et al., 2009; Lundeen et al., 2009; Natarajan et al., 2013). In experiment, a regularized least-square method was used in Brida et al. (2012, 2012) for phase-insensitive detectors. For phase-sensitive detectors, non-diagonal elements can be nonzero and they are usually more challenging to reconstruct. The work in Zhang et al. (2012, 2012) formulated QDT as a convex quadratic optimization problem for this type of detectors. Ref. Wang et al. (2021) proposed a two-stage solution with an analytical computational complexity and error upper bound. Ref. Wang, Dong, and Yonezawa (2019) further studied a binary detector tomography

☆ This research was supported by the National Natural Science Foundation of China (61673264, 62173229), the Australian Government via AUSMURI Grant No. AUSMURI000002, the Australian Research Council Discovery Projects Funding Scheme under Project DP190101566 and U.S. Office of Naval Research Global under Grant N62909-19-1-2129. The material in this paper was partially presented at the 60th IEEE Conference on Decision and Control, December 13-15, 2021, Austin, Texas, USA. This paper was recommended for publication in revised form by Associate Editor Mattia Zorzi under the direction of Editor Torsten Söderström.

* Corresponding authors.
E-mail addresses: xiaoshuixin@sjtu.edu.cn (S. Xiao), wangyuanlong@amss.ac.cn (Y. Wang), daoyidong@gmail.com (D. Dong), zhangjun12@sjtu.edu.cn (J. Zhang).

https://doi.org/10.1016/j.automatica.2022.110296
0005-1098/

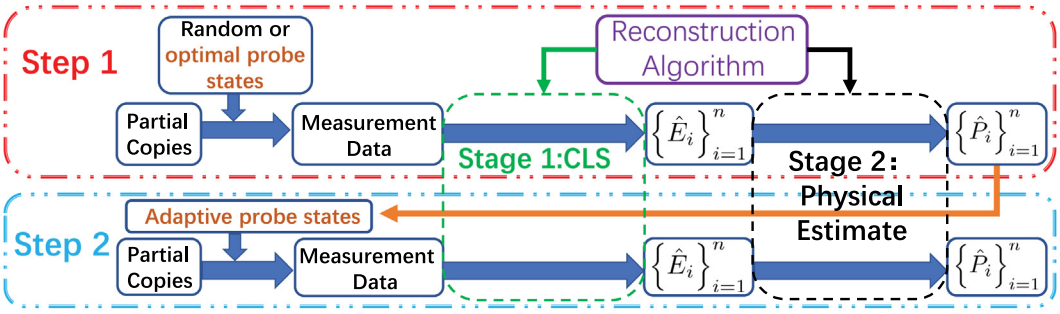

Fig. 1. General procedures for optimal detector tomography and adaptive detector tomography. For optimal detector tomography, we only consider Step 1 and it is non-adaptive. We focus on finding the optimal probe states. For adaptive detector tomography, we choose adaptive probe states in Step 2 based on Step 1 estimation to obtain a more accurate estimate.

method with lower computational complexity by projection. Self-characterization of one-qubit QDT was proposed in Zhang et al. (2020) which does not rely on precisely calibrated probe states.

In this paper, we consider optimal QDT and adaptive QDT which are applicable to both phase insensitive and phase sensitive detectors. The general tomography procedures are shown in Fig. 1. For optimal QDT, we only consider Step 1 where we obtain measurement data and then use the two-stage reconstruction algorithm in Wang et al. (2021) to identify the unknown detectors. A natural question would be which input probe states are optimal, according to some requirements or criteria. Here we use the upper bound of the mean squared error (UMSE) (Wang et al., 2021) and the robustness described by the condition number against measurement errors as two criteria (Xiao, Wang, Dong, & Zhang, 2021). We prove that the minimum UMSE is $\frac{(n-1)(d^4+d^3-d^2)}{4N}$ where d is the dimension of detector matrices, n is the number of detector matrices and N is the resource number (i.e., number of copies of probe states). We also prove the minimum condition number is $\sqrt{d+1}$. We then provide two examples of optimal probe states–SIC (symmetric informationally complete) states with the smallest $M = d^2$ and MUB (mutually unbiased) states for $M = d(d+1)$ where M is the type of probe states. When restricted to product states, we prove the minimum of UMSE is $\frac{20^m(n-1)}{4N}$ and that of the condition number is $3^{\frac{m}{2}}$ where m is the number of qubits.

Another focus we consider is to develop adaptive QDT to enhance the identification accuracy of quantum detectors. Adaptive strategies have been employed in QST and existing results show that adaptive QST has great potential to enhance the estimation precision of quantum states (Huszár & Houlsby, 2012; Kravtsov et al., 2013; Mahler et al., 2013; Pereira, Zambrano, Cortés-Vega, Niklitschek, & Delgado, 2018; Qi et al., 2017; Struchalin et al., 2016). Inspired by adaptive QST, we propose a two-step adaptive QDT as shown in Fig. 1. Step 1 is the same as optimal QDT, and adaptive probe states are chosen in Step 2 based on a rough detector estimation in Step 1. With these adaptive probe states, we can improve the infidelity from $O(1/\sqrt{N})$ to optimal value $O(1/N)$. We also use the superposition of coherent states to realize QDT and use numerical examples to demonstrate the effectiveness of our optimal and adaptive QDT. All proof details of our theoretical results can be found in the extended arXiv version of this paper (Xiao, Wang, Dong & Zhang, 2021).

This paper is organized as follows. In Section 2, we present background knowledge and reconstruction algorithm. In Section 3, we propose optimal QDT and provide concrete examples. In Section 4, we present a two-step adaptive QDT. In Section 5, we give numerical examples of optimal and adaptive QDT. Conclusions are presented in Section 6.

Notation: For a matrix A, $A \geq 0$ means A is positive semidefinite. The conjugation and transpose (T) of A is $A^\dagger$. The trace of A is $\mathrm{Tr}(A)$. The identity matrix is I. The real and complex domains are $\mathbb{R}$ and $\mathbb{C}$, respectively. The tensor product is $\otimes$. The set of all d-dimensional complex/real vectors is $\mathbb{C}^d/\mathbb{R}^d$. Row and column vectors also denoted as $\langle\psi|$ and $|\psi\rangle$, respectively. The Frobenius norm for matrix and 2-norm for vector are $\|\cdot\|$. The Kronecker delta function is δ. $\mathrm{i} = \sqrt{-1}$. The column vectorization function is vec. The diagonal elements of a diagonal matrix $\mathrm{diag}(X)$ are the elements in X and X is a vector. The estimation of variable X denotes $\hat{X}$. For any positive semidefinite $X_{d\times d}$ with spectral decomposition $X = UPU^\dagger$, define $\sqrt{X}$ or $X^{\frac{1}{2}}$ as $U\,\mathrm{diag}\left(\sqrt{P_{11}}, \sqrt{P_{22}}, \ldots, \sqrt{P_{dd}}\right)U^\dagger$. Pauli matrices are $\sigma_x = \left(\begin{smallmatrix} 0 & 1 \\ 1 & 0 \end{smallmatrix}\right)$, $\sigma_y = \left(\begin{smallmatrix} 0 & -\mathrm{i} \\ \mathrm{i} & 0 \end{smallmatrix}\right)$, $\sigma_x = \left(\begin{smallmatrix} 1 & 0 \\ 0 & -1 \end{smallmatrix}\right)$. The fidelity between quantum states ρ and $\hat{\rho}$ is $F_s(\hat{\rho}, \rho) = [\mathrm{Tr}\sqrt{\sqrt{\hat{\rho}}\rho\sqrt{\hat{\rho}}}]^2$.

2. Preliminaries

Here we present the background knowledge and briefly introduce the two-stage QDT reconstruction algorithm in Wang et al. (2021), which will be employed as a critical part for developing optimal QDT.

2.1. Quantum state and measurement

For a d-dimensional quantum system, its state can be described by a $d\times d$ Hermitian matrix ρ, satisfying $\rho \geq 0$, $\mathrm{Tr}(\rho) = 1$. When $\rho = |\psi\rangle\langle\psi|$ for some $|\psi\rangle \in \mathbb{C}^d$, we call ρ a pure state, and its purity $\mathrm{Tr}(\rho^2)$ reaches the maximum value 1. Otherwise, ρ is called a mixed state, and can be represented using pure states $\{|\psi_i\rangle\} : \rho = \sum_i c_i |\psi_i\rangle\langle\psi_i|$ where $c_i \in \mathbb{R}$ and $\sum_i c_i = 1$.

A quantum detector connects the classical and quantum world through a set of operators known as positive-operator-valued measure (POVM). A set of POVM elements is a set of Hermitian and positive semidefinite operators $\{P_i\}$, which is the mathematical representation of quantum detectors, satisfying the completeness constraint $\sum_i P_i = I$. We directly call $\{P_i\}$ a *POVM element* in this paper. The operators P_i may be finite or infinite dimensional in theory. When infinite dimensional, we usually truncate them at a finite dimension d in practice. When ρ is measured using $\{P_i\}$, the probability of obtaining the ith result is given by the Born's rule

$$p_i = \mathrm{Tr}\left(P_i\rho\right). \tag{1}$$

Because of the completeness constraint, we have $\sum_i p_i = 1$. In practical experiments, suppose N (called *resource number*) identical copies of ρ are prepared and the ith result occurs N_i times. Then $\hat{p}_i = N_i/N$ is the experimental estimation of the true value p_i.

2.2. Problem formulation of QDT

By applying known quantum states to an unknown quantum detector and obtaining the measurement results, one can estimate the detector, which is called quantum detector tomography (QDT). Denote the true value of the detector as $\{P_i\}_{i=1}^n$. We design M different types of quantum states (called *probe states*), where each state ρ_j uses the same resource number N/M thus their total number of copies is N. One can formulate the problem of QDT as (Wang et al., 2021):

Problem 1. Given experimental data $\left\{\hat{p}_{ij}\right\}$, solve

$$\min_{\left\{\hat{P}_i\right\}_{i=1}^n} \sum_{i=1}^{n}\sum_{j=1}^{M}\left[\hat{p}_{ij} - \mathrm{Tr}\left(\hat{P}_i\rho_j\right)\right]^2$$

such that $\hat{P}_i = \hat{P}_i^\dagger$, $\hat{P}_i \geq 0$ for $1 \leq i \leq n$ and $\sum_{i=1}^n \hat{P}_i = I$.

There are various methods to formulate and solve the problem of QDT. For maximum likelihood estimation (MLE) (Fiurášek, 2001), if large data are given, the MLE can asymptotically reach the Cramér–Rao bound for parameter estimation while the computational complexity is usually high. There also exist several convex optimization approaches (Feito et al., 2009; Lundeen et al., 2009; Natarajan et al., 2013) which might be more efficient. However, an analytical error upper bound is missing for MLE and convex optimization approaches, making it difficult to optimize the input probe states in the general case without available prior information about the detector. Here we choose the linear regression method due to its simplicity and computational efficiency. Moreover, Ref. Wang et al. (2021) presents the two-stage QDT solution to Problem 1, giving an analytical error upper bound in favor of optimizing general input states. We thus review this solving procedure as follows.

Let $\{\Omega_i\}_{i=1}^{d^2}$ be a complete basis set of orthonormal operators with d-dimension. Without loss of generality, let $\mathrm{Tr}\left(\Omega_i^\dagger\Omega_j\right) = \delta_{ij}$, $\Omega_i = \Omega_i^\dagger$ where $\mathrm{Tr}\left(\Omega_i\right) = 0$ except $\Omega_1 = I/\sqrt{d}$. Then we parameterize the detector and probe states as

$$P_i = \sum_{a=1}^{d^2}\theta_i^a\Omega_a,\ \rho_j = \sum_{b=1}^{d^2}\phi_j^b\Omega_b, \tag{2}$$

where $\theta_i^a \triangleq \mathrm{Tr}\left(P_i\Omega_a\right)$ and $\phi_j^b \triangleq \mathrm{Tr}\left(\rho_j\Omega_b\right)$ are real. Using Born's rule, we can obtain

$$p_{ij} = \sum_{a=1}^{d^2}\phi_j^a\theta_i^a \triangleq \phi_j^T\theta_i, \tag{3}$$

where ϕ_j, θ_i is the parameterization of ρ_j and P_i, respectively. Suppose the outcome for P_i appears n_{ij} times, then $\hat{p}_{ij} = n_{ij}/(N/M)$. Denote the estimation error as $e_{ij} = \hat{p}_{ij} - p_{ij}$. According to the central limit theorem, e_{ij} converges in distribution to a normal distribution with mean zero and variance $\left(p_{ij} - p_{ij}^2\right)/(N/M)$. We thus have the linear regression equation

$$\hat{p}_{ij} = \phi_j^T\theta_i + e_{ij}. \tag{4}$$

Let $\Theta = \left(\theta_1^T, \theta_2^T, \ldots, \theta_n^T\right)^T$ be the vector of all the unknown parameters to be estimated. Collect the parameterization of the probe states as $X = (\phi_1, \phi_2, \ldots, \phi_M)^T$. Let $\hat{y} = (\hat{p}_{11}, \hat{p}_{12}, \ldots, \hat{p}_{1M}, \hat{p}_{21}, \hat{p}_{22}, \ldots, \hat{p}_{2M}, \ldots, \hat{p}_{nM})^T$, $\mathscr{X} = I_n \otimes X$, $e = (e_{11}, e_{12}, \ldots, e_{1M}, e_{21}, e_{22}, \ldots, e_{2M}, \ldots, e_{nM})^T$, $\mathscr{H} = (1, 1, \ldots, 1)_{1\times n} \otimes I_{d^2}$, $d_{d^2\times 1} = (\sqrt{d}, 0, \ldots, 0)^T$. Then the regression equations can be rewritten in a compact form (Wang et al., 2021):

$$\hat{y} = \mathscr{X}\Theta + e, \tag{5}$$

with a linear constraint

$$\mathscr{H}\Theta = d. \tag{6}$$

Now Problem 1 can be transformed into the following equivalent form:

Problem 2. Given experimental data $\hat{y}$, solve $\min_{\left\{\hat{P}_i\right\}_{i=1}^n} \|\hat{y} - \mathscr{X}\hat{\Theta}\|^2$ such that $\mathscr{H}\hat{\Theta} = d$ and $\hat{P}_i \geq 0$ for $1 \leq i \leq n$, where $\hat{\Theta}$ is the parameterization of $\left\{\hat{P}_i\right\}$.

In Wang et al. (2021), Problem 2 is split into two approximate subproblems:

Problem 2.1. Given experimental data $\hat{y}$, solve $\min_{\left\{\hat{E}_i\right\}_{i=1}^n} \|\hat{y} - \mathscr{X}\hat{\Theta}\|^2$ such that $\mathscr{H}\hat{\Theta} = d$ where $\hat{\Theta}$ is the parameterization of $\left\{\hat{E}_i\right\}$.

Problem 2.2. Given $\sum_{i=1}^n \hat{E}_i = I$, solve $\min_{\left\{\hat{P}_i\right\}_{i=1}^n} \sum_{i=1}^n \left\|\hat{E}_i - \hat{P}_i\right\|^2$ such that $\sum_{i=1}^n \hat{P}_i = I$ and $\hat{P}_i \geq 0$ for $1 \leq i \leq n$.

The reconstruction algorithm has two stages, as shown in Fig. 1. In Stage 1, Problem 2.1 is solved by Constrained Least Squares (CLS) method and the form of the solution is further simplified. In Stage 2, Problem 2.2 is solved by matrix decomposition. We briefly review the two-stage QDT reconstruction algorithm in Wang et al. (2021) in the next subsection.

2.3. Two-stage QDT reconstruction algorithm

In Stage 1, we directly give the simplified form of the CLS solution to Problem 2.1 as

$$\hat{\Theta}_{\mathrm{CLS}} = \begin{pmatrix} \left(X^TX\right)^{-1}X^T\left(\hat{y}_1 - \frac{1}{n}y_0\right) + \frac{1}{n}d \\ \vdots \\ \left(X^TX\right)^{-1}X^T\left(\hat{y}_n - \frac{1}{n}y_0\right) + \frac{1}{n}d \end{pmatrix}, \tag{7}$$

where $\hat{y}_i = \left(\hat{p}_{i1}, \hat{p}_{i2}, \ldots, \hat{p}_{iM}\right)^T$ for $1 \leq i \leq n$ and $y_0 = ((1, \ldots, 1)_{1\times M})^T = \sum_i \hat{y}_i$. Let the ith block be $\hat{\Theta}_{i,\mathrm{CLS}} = \left(\hat{\theta}_i^1, \ldots, \hat{\theta}_i^{d^2}\right)^T$ and the Stage 1 estimate is $\hat{E}_i = \sum_{a=1}^{d^2}\hat{\theta}_i^a\Omega_a$ which may have negative eigenvalues. Thus, Stage 2 is designed to obtain a physical estimate $\hat{P}_i$ by eigenvalue correction with three substages. Firstly, we decompose $\hat{E}_i = \hat{F}_i - \hat{G}_i$ with $\hat{F}_i \geq 0$, $\hat{G}_i \geq 0$. We then perform a spectral decomposition to obtain $\hat{E}_i = \hat{R}_i\hat{K}_i\hat{R}_i^\dagger$. Assume there are $\hat{n}_i$ nonpositive eigenvalues for $\hat{E}_i$, and they are in decreasing order. Thus, the best decomposition in the sense of minimizing $\|\hat{G}_i\|$ is $\hat{F}_i = \hat{R}_i\mathrm{diag}((\hat{K}_i)_{11}, (\hat{K}_i)_{22}, \ldots, (\hat{K}_i)_{(d-\hat{n}_i)(d-\hat{n}_i)}, 0, \ldots, 0)\hat{R}_i^\dagger$, and $\hat{G}_i = -\hat{R}_i\mathrm{diag}(0, \ldots, 0, (\hat{K}_i)_{(d-\hat{n}_i+1)(d-\hat{n}_i+1)}, (\hat{K}_i)_{(d-\hat{n}_i+2)(d-\hat{n}_i+2)}, \ldots, (\hat{K}_i)_{dd})\hat{R}_i^\dagger$. Secondly, we apply decomposition $I + \sum_i \hat{G}_i = \sum_i \hat{F}_i = \hat{C}\hat{C}^\dagger$, and hence $\sum_i \hat{C}^{-1}\hat{F}_i\hat{C}^{-\dagger} = I$. Let $\hat{B}_i = \hat{C}^{-1}\hat{F}_i\hat{C}^{-\dagger}$ which is positive semidefinite and $\sum_i \hat{B}_i = I$. For any unitary $\hat{U}$, $\hat{C}\hat{C}^\dagger = \hat{C}\hat{U}\hat{U}^\dagger\hat{C}^\dagger$ holds. Therefore, $\hat{U}^\dagger\hat{B}_i\hat{U}$ can also be an estimate of the detector. To neutralize the effect of $\hat{U}^\dagger\hat{C}^{-1}(\cdot)(\hat{C}^\dagger)^{-1}\hat{U}$ on $\hat{F}_i$, we define an optimal unitary matrix $\hat{U}_{\mathrm{op}}$ to minimize $\|\hat{C}\hat{U}_{\mathrm{op}} - I\|$ (Wang et al., 2021) and its analytical expression is $\hat{U}_{\mathrm{op}} = \sqrt{\hat{C}^\dagger\hat{C}}\hat{C}^{-1}$. Therefore, the final estimate is $\hat{P}_i = \hat{U}_{\mathrm{op}}^\dagger\hat{B}_i\hat{U}_{\mathrm{op}}$. This general algorithm can be used for arbitrary $n \geq 2$.

3. Optimal quantum detector tomography

In detector tomography as shown in Step 1 in Fig. 1, a natural way to reduce the tomography error is to carefully choose the probe states according to a certain optimality criterion, which should be independent of the detector. In this section, we propose a criterion based on two non-conflicting indices (UMSE and condition number), subsequently present the conditions on achieving optimal detector tomography and provide illustrative examples.

3.1. Optimality criterion

One index to evaluate probe states is to score their worst performance, i.e., their upper bounds of estimation errors. Let $\mathbb{E}$ denote the expectation w.r.t. all possible measurement results. The Stage 1 error $\left\|\hat{E}_i - P_i\right\|$ between the estimate $\hat{E}_i$ and its true value P_i is bounded by UMSE (upper bound of the mean squared error) (Wang et al., 2021)

$$\begin{aligned}\mathbb{E}\left(\sum_i \left\|\hat{E}_i - P_i\right\|^2\right) &= \mathbb{E}\left(\left\|\hat{\Theta}_{\mathrm{CLS}} - \Theta\right\|^2\right)\\ &\le \frac{(n-1)M}{4N}\operatorname{Tr}\left[(X^TX)^{-1}\right],\end{aligned} \tag{8}$$

and the final estimation error for all detectors $\mathbb{E}\left(\Sigma_i \left\|\hat{P}_i - P_i\right\|^2\right)$ is bounded by (Wang et al., 2021)

$$\begin{aligned}&\mathbb{E}\left(\sum_i \left\|\hat{P}_i - P_i\right\|^2\right)\\ \le&\frac{(dn + 2\sqrt{d}n + 1)(n-1)M}{4N}\operatorname{Tr}\left[(X^TX)^{-1}\right] + o\left(\frac{1}{N}\right).\end{aligned} \tag{9}$$

Since in (8) and (9) the parts dependent on probe states are both $M\operatorname{Tr}\left[(X^TX)^{-1}\right]$, we take it as our first criterion. For general QDT, we have no special prior knowledge on the detectors, and the following conditions are equivalent: (i) the detector cannot be uniquely identified; (ii) the probe states do not span the space of all d-dimensional states; (iii) X^TX is singular; (iv) the UMSE is infinite. From (i) and (iv), it is thus reasonable to take $M\operatorname{Tr}(X^TX)^{-1}$ as an evaluation index. We require the optimal probe states to minimize $M\operatorname{Tr}(X^TX)^{-1}$. This criterion is conservative and its limitation is that the UMSE might not be tight. The relation (8) is only tight for the case $P_1 = P_2 = I/2$ and (9) is always loose. Therefore, minimizing UMSE is not equivalent to minimizing MSE. In addition, UMSE depends on the assumption that there only exists statistics error in the measurement data from finite state copies (discussed in Remark 4). Despite these limitations, numerical results in Wang et al. (2021) (e.g., Fig. 4 therein) indicate a very similar behavior between UMSE and MSE when changing the probe states while maintaining the other parameters n, M, N fixed. Hence, UMSE is also a useful index evaluating the probe state set.

The second index we consider is, for a set of probe states, how robust the generated estimation result is w.r.t. measurement noise. Note that our CLS estimation (7) is in fact equivalent to the least squares estimation of the linear regression problem

$$\begin{pmatrix}\hat{y}_1 - \frac{1}{n}y_0\\ \vdots\\ \hat{y}_n - \frac{1}{n}y_0\end{pmatrix} = (I_n \otimes X)\begin{pmatrix}\Theta_1 - \frac{1}{n}d\\ \vdots\\ \Theta_n - \frac{1}{n}d\end{pmatrix}. \tag{10}$$

Typically, the sensitivity of a linear system solution to perturbations in the data is evaluated by the condition number of the coefficient matrix, defined (among several possible choices) in this paper as $\operatorname{cond}(A) = \frac{\sigma_{\max}(A)}{\sigma_{\min}(A)}$, where $\sigma_{\max/\min}(A)$ is the maximum/minimum singular value of A. Hence, to maximize the estimation robustness w.r.t. measurement noise amounts to minimizing the condition number in (10) $\operatorname{cond}(I_n \otimes X) = \operatorname{cond}(I_n)\operatorname{cond}(X) = \operatorname{cond}(X)$. Therefore, the second evaluation index is chosen as $\operatorname{cond}(X)$. To sum up, the optimal probe states should minimize $M\operatorname{Tr}(X^TX)^{-1}$ and minimize $\operatorname{cond}(X)$ *simultaneously*. In the following we give specific characterization and show that the two optimal indices can be achieved simultaneously for several examples.

3.2. Optimal probe states

We now give the condition on optimal probe states (*OPS*).

Theorem 1. *For a d-dimensional detector with n matrices, assume each type of probe states has the same number of copies, altogether summed to N copies. Then the minimum of UMSE is $\frac{(n-1)(d^4+d^3-d^2)}{4N}$ and the minimum of $\operatorname{cond}(X)$ is $\sqrt{d+1}$. These minima are achieved simultaneously if and only if there exist M different types of probe states such that X^TX is diagonal and its eigenvalues are $\lambda_1 = \frac{M}{d}$ and $\lambda_2 = \cdots = \lambda_{d^2} = \frac{M}{d(d+1)}$.*

Our results also show that the description of OPS in Assumption 1 in Wang et al. (2021) needs to be more precise. For certain M, if there exist OPS, all of them must be pure states because $\sum_{j=1}^{M}\operatorname{Tr}(\rho_j^2) = \sum_{j=1}^{d^2}\lambda_i = M$. This indicates that pure states are better than mixed states. However, it is not clear whether these OPS exist for arbitrary $M \ge d^2$. Thus, whether we can always find a pure state set which is better than arbitrary mixed state set for given M is still an open problem.

Remark 1. In system identification, the similar problem called input design problem has been widely discussed. There are many existing results, e.g., D,A,E-optimal input design (Boyd & Vandenberghe, 2004). The common idea behind the problem of our optimal probe states and optimal input design is that both problems consider minimizing the trace of the covariance matrix, which is A-optimal input design (Boyd & Vandenberghe, 2004). The difference is that we also consider robustness and other physical eigenvalue constraints (e.g., purity) for probe states. Thus, we cannot directly adapt classical input design problem for the quantum case.

Remark 2. If we only want to reach the minimum condition number $\sqrt{d+1}$ without considering UMSE, we need to ensure $\frac{\lambda_1}{\lambda_{d^2}} = d+1$ which can be satisfied even for mixed states. For example, for a concentric sphere inside the Bloch sphere, we can also find the corresponding platonic solid on it which has the smallest condition number $\sqrt{d+1}$ (this case will be discussed later). Therefore, if we only consider minimum condition number, we cannot obtain the minimum UMSE. However, if we only consider minimum UMSE, the eigenvalues also satisfy the requirement of minimum condition number. Hence, when we solve the optimization problem and analyze optimal probe states, it suffices to only consider minimum UMSE.

Remark 3. In quantum state tomography, the condition number for the optimal measurement is 1, achieved by special measurement such as the optimal generalized Pauli operators (Miranowicz et al., 2014). However, in QDT, OPS need to satisfy the unit-trace constraint. Therefore, the largest eigenvalue λ_1 must be equal to or larger than $\frac{M}{d}$ and the minimum condition number is $\sqrt{d+1}$.

Remark 4. We consider two criteria for optimization—upper bound of the mean squared error (UMSE) and the robustness described by the condition number. For UMSE, we assume there only exists statistics error from finite state copies and the analytical upper bound depends on this assumption. If this assumption is not satisfied, the UMSE should be adjusted by adding the unmodeled noise (e.g., apparatus noise) to the error ϵ in (5). For robustness, condition number characterizes the sensitivity of the estimation result to errors in measurement data. Hence, this criterion is unrelated to the specific sources of the errors.

We then give two examples of OPS for $M = d^2$ and $M = d(d+1)$ which are motivated by projection measurements.

The first example is motivated from SIC-POVM. To reconstruct an unknown quantum state ρ, a generalized measurement must have at least d^2 linear independent elements, which is called informationally complete. Furthermore, if the measurement results are maximally independent, the POVM is called symmetric informationally complete POVM (SIC-POVM). The simplest mathematical definition of an SIC-POVM is a set of d^2 normalized vectors $|\phi_k\rangle$ in $\mathbb{C}^d$ satisfying (Renes, Blume-Kohout, Scott, & Caves, 2004)

$$\left|\langle\phi_j|\phi_k\rangle\right|^2 = \frac{1}{d+1}, \quad j \neq k. \tag{11}$$

It has been conjectured that SIC-POVMs exist for all dimensions (Renes et al., 2004) and their existence has been given for $d \leq 121$, and some other sporadic values (Scott, 2017). When SIC-POVMs exist in d dimension, we define the d^2 pure states $|\phi_k\rangle \in \mathbb{C}^d (1 \leq k \leq d^2)$ to be *SIC states* if they satisfy (11). Then we have the following conclusion.

Proposition 1. *d-dimensional SIC states (when they exist) are a set of OPS with the smallest M as $M = d^2$.*

The second example is motivated from MUB measurement. Two sets of orthogonal bases $\mathscr{B}^k = \{|\psi_i^k\rangle : i = 1, \ldots, d\}$ and $\mathscr{B}^\ell = \{|\psi_j^\ell\rangle : j = 1, \ldots, d\}$ are called mutually unbiased if and only if (Adamson & Steinberg, 2010)

$$\left|\langle\psi_i^k|\psi_j^\ell\rangle\right|^2 = \begin{cases} 1/d & \text{for } k \neq \ell, \\ \delta_{i,j} & \text{for } k = \ell. \end{cases} \tag{12}$$

In particular, one can find maximally $d+1$ sets of mutually unbiased bases in Hilbert spaces of prime-power dimension $d = p^k$, with p a prime and k a positive integer (Durt, Englert, Bengtsson, & Życzkowski, 2010). When $d+1$ sets of MUB measurement exist in $\mathbb{C}^d$, we view each projective MUB measurement operator as a pure state and we call them *MUB states*. Thus, MUB states always exist for m-qubit systems ($d = 2^m$). Then we have the following conclusion.

Proposition 2. *d-dimensional MUB states (when they exist) are a set of OPS for $M = d(d+1)$.*

For $M \neq d^2$ and $M \neq d(d+1)$, we leave it an open problem when there always exist OPS satisfying the two indices simultaneously. For two-qubit detectors, from the above results we know the optimal probe states can be constructed using 4-dimensional MUB states and SIC states as shown in Appendix A in Xiao, Wang et al. (2021). A similar two-qubit problem for QST was discussed in Qi et al. (2013) to determine the optimal measurement based on UMSE and in Miranowicz et al. (2014) based on condition number.

For one-qubit probe states, they have simple geometric property; i.e., they are in the Bloch sphere. The pure states are on the surface and the mixed states are inside the sphere. Hence, an alternative method to search for one-qubit OPS is based on geometric symmetry. For $M = 4$, when the probe states are on the surface of Bloch sphere and become the four vertices of a tetrahedron concentric with Bloch sphere, they are OPS. In fact, they are also SIC states. For $M = 6$, one can construct OPS similarly using octahedron, and they are also MUB states. We also have cube, icosahedron, dodecahedron for $M = 8, 12, 20$, respectively, which are OPS. We conjecture all one-qubit OPS are constructed from the five platonic solids on the Bloch sphere in this way, and we show there do not exist OPS for $M = 5$ in Appendix B in Xiao, Wang et al. (2021). For multi-qubit states, we still do not fully know the geometric property and it is thus an open problem to find other optimal probe states.

3.3. Product probe state

In experiment, product states are among the ones most straightforwardly to be implemented. In this subsection we consider the case $d = 2^m$ for some integer m and each probe state is an m-qubit tensor product state as $\rho_j = \rho_{j_1}^{(1)} \otimes \cdots \otimes \rho_{j_m}^{(m)}$ where $1 \leq j_1 \leq M_1, \ldots, 1 \leq j_m \leq M_m$ and there are M_i different types of one-qubits for the ith qubit of the product states. The total number of these m-qubit tensor product states is thus $\prod_{i=1}^m M_i$. We then give their optimal UMSE and condition number.

Theorem 2. *The minimum UMSE of m-qubit product probe state is $\frac{20^m(n-1)}{4N}$ and the minimum condition number is $\sqrt{3^m}$. These minima are achieved simultaneously if and only if each qubit is among optimal one-qubit states.*

Here we compare the two criteria—UMSE and condition number between OPS and optimal product states for an m-qubit detector with the dimension $d = 2^m$. The UMSEs are $\frac{(n-1)(16^m+8^m-4^m)}{4N}$ for OPS and $\frac{20^m(n-1)}{4N}$ for optimal product states. UMSE of optimal probe states is always smaller than that of optimal product states for $m \geq 2$. For $m = 1$, they are both $\frac{20(n-1)}{4N}$. For condition number, it is $\sqrt{2^m+1}$ for OPS and $\sqrt{3^m}$ for optimal product states. Thus, for both UMSE and condition number, OPS play better than optimal product states in multi-qubit systems. Because most of the OPS are entangled states, this is an example showcasing the advantage of entanglement in QDT.

We give an example of optimal two-qubit product probe states. The detailed derivation is shown in Xiao, Wang et al. (2021) and the optimization problem is

$$\begin{aligned} \min \ & \sum_{i=1}^{16} \frac{M}{\lambda_i} \\ \text{s.t.} \ & \sum_{i=1}^{16} \lambda_i = M, \lambda_1 \geq \frac{M}{4}, \\ & \sum_{i=1}^{4} \lambda_i \geq \frac{M}{2}, \sum_{i=1}^{7} \lambda_i \geq \frac{3M}{4}. \end{aligned} \tag{13}$$

It can be proven that $\sum_{i=1}^{16} \frac{M}{\lambda_i}$ reaches its minimum 400 and the minimum UMSE is $\frac{100(n-1)}{N}$ when $\lambda_1 = \frac{M}{4}, \lambda_2 = \cdots = \lambda_7 = \frac{M}{12}, \lambda_8 = \cdots = \lambda_{16} = \frac{M}{36}$. It can be verified that this minimum UMSE can be reached by using the tensor of platonic solid states such as $M = 36$ (Cube). The minimum condition number is $\sqrt{\frac{\lambda_1}{\lambda_{16}}} = \sqrt{\frac{M/4}{M/36}} = 3$.

3.4. Superposition of coherent probe state

In quantum optics experiments, the preparation of number states (or Fock states) $|k\rangle (k \in \mathbb{N})$ is usually a difficult task,

especially when k is large. Therefore, it is also difficult to prepare SIC and MUB states. Coherent states, more straightforward to be prepared, are more commonly used as probe states for QDT in practice. Thus, a good approach is to use the superposition of several coherent states to approximate SIC states and MUB states.

A coherent state is denoted as $|\alpha\rangle$ where $\alpha \in \mathbb{C}$ and it can be expanded using number states as

$$|\alpha\rangle = e^{-\frac{|\alpha|^2}{2}} \sum_{i=0}^{\infty} \frac{\alpha^i}{\sqrt{i!}} |i\rangle. \tag{14}$$

The inner product relationship between two states $|\alpha\rangle$ and $|\beta\rangle$ is

$$\langle\beta|\alpha\rangle = \mathrm{e}^{-\frac{1}{2}\left(|\beta|^2+|\alpha|^2-2\beta^*\alpha\right)}. \tag{15}$$

Let $|\alpha_d\rangle = \mathrm{e}^{-\frac{|\alpha|^2}{2}} \sum_{i=0}^{d-1} \frac{\alpha^i}{\sqrt{i!}} |i\rangle$. Coherent states are in essence infinite dimensional. To estimate a d-dimensional detector, we employ $|\alpha_d\rangle$ as the approximate description of $|\alpha\rangle$, and we assume that the discarded part $|\alpha\rangle - |\alpha_d\rangle$ has a small enough influence such that it can be neglected. A matrix or vector with subscript d means it is truncated in d dimension.

Remark 5. It can lead to significant error to approximate a general pure state using only one coherent state instead of the superposition of many. This problem is often referred to as the nonclassicality of states. As an example, we now consider a Fock state $|n\rangle$. The infidelity is

$$1 - F_s(|n\rangle\langle n|, |\alpha\rangle\langle\alpha|) = \left[2\left(1 - \exp(-|\alpha|^2)\frac{|\alpha|^{2n}}{n!}\right)\right]^{1/2}.$$

The minimum infidelity is obtained by $|\alpha|^2 = n$ and for $n = 0, 1, 2$, the minimum infidelity is $0, 0.6321, 0.7293$, respectively. Thus, the distance between one Fock state and one coherent state may be quite large. This also shows that the Fock state $|n\rangle$ becomes more and more non-classical as the value n increases (Wünsche, Dodonov, Man'ko, & Man'ko, 2001).

In *quantum state engineering*, a central problem is how to construct a pure state by superposition of coherent states. There are two main approaches to do this. One is to write the pure state as a superposition of coherent states along the real axis in phase space

$$|\psi\rangle = \int_{-\infty}^{\infty} \mathscr{F}(\alpha)|\alpha\rangle d\alpha, \tag{16}$$

where $\mathscr{F}(\alpha)$ is the distribution function. The other choice is the superposition on a circle

$$|\psi\rangle = \int_0^{2\pi} \mathscr{F}_R(\phi)\left|Re^{i\phi}\right\rangle d\phi, \tag{17}$$

where R is the radius of the circle and $\mathscr{F}_R(\phi)$ a circle distribution function. The analytical solutions of $\mathscr{F}(\alpha)$ and $\mathscr{F}_R(\phi)$ were given in Szabo, Adam, Janszky, and Domokos (1996). They also gave the discrete superposition of coherent states to construct pure states by discretizing the above equations. Ref. Janszky, Domokos, Szabó, and Adam (1995) evaluated the performance to construct squeezed displaced number states and Szabo et al. (1996) gave a representation of a Fock state $|n\rangle$ by $n+1$ coherent states. If we can construct all Fock states with high accuracy, we can use these Fock states to construct all the ideal pure states we need. However, in practice, the technique to superpose many coherent states arbitrarily is still developing.

In this paper, we use the finite superposition of s coherent states $|\tilde{\psi}\rangle = \sum_{k=1}^{s} c_k |\alpha_d\rangle_k$ to approximate an ideal pure state $|\psi\rangle$ where $|\tilde{\psi}\rangle$ indicates that it has not been normalized. Hence, $|\tilde{\psi}\rangle$ is not yet a quantum state in the most strict sense. To find the superposition state $|\tilde{\psi}\rangle$, at first sight it can be formulated as an optimization problem to maximize fidelity as

$$\max_{|\tilde{\psi}\rangle} |\langle\psi|\tilde{\psi}\rangle|^2, \tag{18}$$

since the fidelity is $F_s(\hat{\rho}, \rho) = [\mathrm{Tr}\sqrt{\sqrt{\hat{\rho}}\rho\sqrt{\hat{\rho}}}]^2 = |\langle\psi|\tilde{\psi}\rangle|^2$. However, for the purpose of QDT, this cost function is not the most suitable. The most important part of the superposed state $|\tilde{\psi}\rangle$ is its direction. We hope to align it in the same direction as $|\psi\rangle$, even if the norm$\||\tilde{\psi}\rangle\|$ can be different from $\||\psi\rangle\| = 1$. Hence, we need the normalized state $\frac{|\tilde{\psi}\rangle}{\sqrt{\langle\tilde{\psi}|\tilde{\psi}\rangle}}$ to be a good approximation to $|\psi\rangle$, which thus leads to the numerator of (19). Also, if $\||\tilde{\psi}\rangle\|$ is too small, we cannot neglect elements in the dimension larger than d and the corresponding measurement data $\mathrm{Tr}\left(\left|\tilde{\psi}\right\rangle\left\langle\tilde{\psi}\right| P_i\right)$ will be small, leading to low measurement accuracy for given the same resource number N. Therefore, we add a penalty $\langle\tilde{\psi}|\tilde{\psi}\rangle$ to prevent the norm $|\tilde{\psi}\rangle$ from being too small. Thus, we design a new cost function as

$$\min_{|\tilde{\psi}\rangle} \frac{\left\| \frac{|\tilde{\psi}\rangle}{\sqrt{\langle\tilde{\psi}|\tilde{\psi}\rangle}} - |\psi\rangle \right\|^2}{\langle\tilde{\psi}|\tilde{\psi}\rangle}. \tag{19}$$

This optimization problem is usually non-convex, and thus we select different initial points and numerically search for the best solution.

3.5. Error analysis for state preparation

When we prepare probe states such SIC states and MUB states in experiment, there usually exist state preparation errors. For example, if we use superposition of coherent states, there exists approximation error between the ideal target probe state and the superposition of coherent states when the number of coherent states for superposition is not large enough. We give the error analysis on UMSE and condition number when there exists state preparation error (see Appendix C in Xiao, Wang et al. (2021) for the proof detail).

Theorem 3. *Given two probe state sets* $\{\rho_j\}_1^M$ *and* $\{\hat{\rho}_j\}_1^M$, *if* $\max_j \|\rho_j - \hat{\rho}_j\| \le \varepsilon$ *and* $\varepsilon \le \frac{\lambda_{d^2}}{2M}$, *the corresponding error in* $\frac{(n-1)M}{4N}$ $\left|\mathrm{Tr}\left(X^TX\right)^{-1} - \mathrm{Tr}\left(\hat{X}^T\hat{X}\right)^{-1}\right|$ *is upper bounded by* $\frac{2(n-1)d^2M^2\varepsilon}{4N\left(\lambda_{d^2} - 2M\varepsilon\right)^2}$ *where* $\lambda_{d^2} > 0$ *is the smallest eigenvalue of the parameterization matrix* X^TX *and the corresponding error on condition number is upper bounded by* $\frac{M\left(\lambda_1 + \lambda_{d^2}\right)\varepsilon}{\left(\lambda_{d^2} - 2M\varepsilon\right)^2}$ *where* λ_1 *is the largest eigenvalue of* X^TX.

4. Adaptive detector tomography

As shown in Fig. 1, after employing partial resources to obtain a rough estimate of the detector through Step 1, one can design new probe states dependent on the specific estimation value of the detector to further improve the accuracy in Step 2. Our adaptive QDT scheme is applicable for arbitrary reconstruction algorithm.

4.1. Evaluation index

In quantum information, fidelity (or infidelity) has profound physical meaning to characterize the distance and similarity between two quantum states (or operations). It has been a widely

used metric (Hübner, 1992; Jozsa, 1994; Nielsen & Chuang, 2010). In developing adaptive QDT, we also employ infidelity as the evaluation index.

The fidelity between two arbitrary states $\hat{\rho}$ and ρ is defined by

$$F_s(\hat{\rho}, \rho) \triangleq [\mathrm{Tr}\sqrt{\sqrt{\hat{\rho}}\rho\sqrt{\hat{\rho}}}]^2, \tag{20}$$

which has three basic properties:

$$(i)\ \ F_s(\hat{\rho}, \rho) = F_s(\rho, \hat{\rho}); \tag{21}$$

$$(ii)\ \ 0 \le F_s(\hat{\rho}, \rho) \le 1; \tag{22}$$

$$(iii)\ \ F_s(\hat{\rho}, \rho) = 1 \ \Leftrightarrow\ \ \hat{\rho} = \rho. \tag{23}$$

To extend the fidelity definition from states to detectors, a natural idea is to normalize the POVM element such that it has the same mathematical property as a quantum state. This leads to the definition

$$F_0\left(\hat{P}_i, P_i\right) \triangleq \left[\mathrm{Tr}\sqrt{\sqrt{\hat{P}_i}P_i\sqrt{\hat{P}_i}}\right]^2 / \left[\mathrm{Tr}\left(P_i\right)\mathrm{Tr}\left(\hat{P}_i\right)\right]. \tag{24}$$

This definition has been widely used in QDT (Feito et al., 2009; Lundeen et al., 2009; Zhang, Datta et al., 2012) to evaluate the estimation performance, and corresponding infidelity is defined as $1 - F_0\left(\hat{P}_i, P_i\right)$. However, we find that this definition is not always appropriate, because in certain circumstances the third property (23) does not hold for (24) (we call this phenomenon *distortion*). More specifically, for certain detector $\{P_i\}_{i=1}^n$, *distortion* means there exists $\left\{\hat{P}_i\right\}_{i=1}^n$ such that $F_0\left(\hat{P}_i, P_i\right) = 1$ for all $1 \le i \le n$ while $\hat{P}_i = P_i$ fails for at least one i. For example, suppose the detector is $P_1 = P_2 = P_3 = \frac{I}{3}$ and the estimations are $\hat{P}_1 = a_1P_1$, $\hat{P}_2 = a_2P_2$, $\hat{P}_3 = a_3P_3$ where a_1, a_2 and a_3 are three arbitrary positive numbers satisfying $a_1+a_2+a_3 = 3$. The fidelities for the three detectors are all maximum 1, but the estimation is in fact usually not accurate. We characterize when the evaluation index (24) will distort in the following proposition whose proof can be found in Appendix D in Xiao, Wang et al. (2021).

Proposition 3. *The evaluation index (24) will distort if and only if $\{P_i\}_{i=1}^n$ are linearly dependent, i.e., there exists nonzero $c \in \mathbb{R}^n$ such that $\sum_{i=1}^n c_iP_i = 0$. Specially, if $d^2 < n$, there must exist distortion.*

When distortion happens, $\lim_{F_0(\hat{P}_i,P_i)\to 1}\hat{P}_i = P_i$ fails. That is, the estimation can be on a wrong track even if the fidelity approaches to 1. To fix this problem, we add $\left[\mathrm{Tr}(P_i - \hat{P}_i)\right]^2/d^2$ and propose a new detector fidelity as

$$\begin{aligned} F\left(\hat{P}_i, P_i\right) = &\left[\mathrm{Tr}(\sqrt{\sqrt{\hat{P}_i}P_i\sqrt{\hat{P}_i}})\right]^2 / \left[\mathrm{Tr}\left(P_i\right)\mathrm{Tr}\left(\hat{P}_i\right)\right] \\ &- \left[\mathrm{Tr}\left(P_i - \hat{P}_i\right)\right]^2/d^2. \end{aligned} \tag{25}$$

The fidelity (25) takes values in $(\frac{1}{d}-1, 1]$ and we give the proof of the lower bound in Appendix E in Xiao, Wang et al. (2021). When $F\left(\hat{P}_i, P_i\right) = 1$, we must have $\hat{P}_i = P_i$ (and vice versa), solving the distortion problem of (24). For the rest of this paper, we refer to "fidelity" as (25), unless otherwise declared. The infidelity is defined as $1 - F\left(\hat{P}_i, P_i\right)$.

4.2. Two-step adaptive quantum detector tomography

Let $\{|\lambda_t\rangle\}$ be the eigenvectors of P_i for given i, where the zero eigenvalues are $\lambda_{r+1} = \cdots = \lambda_d = 0$. We can view $\frac{P_i}{\mathrm{Tr}(P_i)}$ and $\frac{\hat{P}_i}{\mathrm{Tr}\left(\hat{P}_i\right)}$ as two quantum states. Thus, we may use the analysis in Pereira et al. (2018) to obtain the Taylor series expansion of the new infidelity $1 - F(\hat{P}_i, P_i)$ based on (25) up to the second order as

$$\begin{aligned} &\mathbb{E}\left(1 - F(\hat{P}_i, P_i)\right) \\ =&\mathbb{E}\left(1 - F_0\left(\hat{P}_i, P_i\right) + \left[\mathrm{Tr}\left(P_i - \hat{P}_i\right)\right]^2/d^2\right) \\ =&\mathbb{E}\left(1 - F_0\left(\hat{P}_i, P_i\right) + \left(\sum_{t=1}^d \langle\lambda_t|\Delta_2|\lambda_t\rangle\right)^2/d^2\right) \\ =&\mathbb{E}\left(\sum_{t=r+1}^d \langle\lambda_t|\Delta_1|\lambda_t\rangle\right) + \mathbb{E}\left(\frac{1}{2}\sum_{t,k=1}^r \frac{|\langle\lambda_t|\Delta_1|\lambda_k\rangle|^2}{\lambda_t+\lambda_k}\right) \\ &- \mathbb{E}\left(\frac{1}{4}\left[\sum_{t=r+1}^d \langle\lambda_t|\Delta_1|\lambda_t\rangle\right]^2\right) \\ &+ \mathbb{E}\left(\sum_{t=1}^d\sum_{k=1}^d \langle\lambda_t|\Delta_2|\lambda_t\rangle\langle\lambda_k|\Delta_2|\lambda_k\rangle/d^2\right) + O\left(\|\Delta_1\|^3\right), \end{aligned} \tag{26}$$

where $\Delta_1 = \frac{P_i}{\mathrm{Tr}(P_i)} - \frac{\hat{P}_i}{\mathrm{Tr}\left(\hat{P}_i\right)}$, $\Delta_2 = P_i - \hat{P}_i$. Crucially, the new term $-\left[\mathrm{Tr}\left(P_i - \hat{P}_i\right)\right]^2/d^2$ is in the second order instead of in the first order, and we can thus imitate the analysis for QST in Pereira et al. (2018). Note that we use a perturbation method thus (26) is valid only around P_i. The condition can be guaranteed because we are analyzing the asymptotic behavior as N tends to infinity (large enough).

According to the Taylor series, the scaling performance of the infidelity depends on the rank of the detector. For instance, for a full-rank POVM element, the first-order term vanishes and the infidelity scales as $O(1/N)$ using just non-adaptive QDT. For a rank deficient P_i, the first-order term dominates and thus the infidelity scales as $O(1/\sqrt{N})$ by QDT which only has Step 1 in Fig. 1. The optimal scaling of infidelity $1 - F_s(\hat{\rho}, \rho)$ is $O(1/N)$ for unbiased estimate in QST (Zhu, 2012) and the optimal scaling of $-\left[\mathrm{Tr}\left(P_i - \hat{P}_i\right)\right]^2/d^2$ is always not worse than $O(1/N)$. Thus, the optimal scaling of infidelity $1 - F_0(\hat{P}_i, P_i)$ or $1 - F(\hat{P}_i, P_i)$ is also $O(1/N)$. From Pereira et al. (2018), we know the second-order terms always scale as $O(1/N)$. Therefore, for rank-deficient detectors, the behavior of the infidelity can be corrected to $O(1/N)$ if one can eliminate the influence of the first-order term (Pereira et al., 2018). This depends on the diagonal coefficients of Δ_1 in the kernel of $\frac{P_i}{\mathrm{Tr}(P_i)}$, which suggests performing QDT in a basis aligning with the eigenvectors of P_i (Pereira et al., 2018).

The detailed adaptive procedure is as follows. To simplify the expression, we use P to represent each POVM element P_i. For P, given a probe state set $\{\rho_j\}_{j=1}^M$, we choose one among them (e.g., ρ_a) and its spectral decomposition is $\rho_a = V_a\Gamma_aV_a^\dagger$. The spectral decomposition of P_i is $P = U\Lambda U^\dagger$. To perform QDT in a basis that agrees with the eigenvectors of P (Pereira et al., 2018), we change each probe state ρ_j to $\tilde{\rho}_j$ by a common conjugation as

$$\tilde{\rho}_j = UV_a^\dagger\rho_jV_aU^\dagger. \tag{27}$$

However, in practice, we do not know U_i. Therefore, we have two steps as shown in Fig. 1. In Step 1, we obtain an estimator $\left\{\tilde{P}\right\}$ by applying non-adaptive QDT on an ensemble of size N_0. Then in Step 2, we use new probe states $\tilde{\rho}_j$ as

$$\tilde{\rho}_j = \tilde{U} V_a^\dagger \rho_j V_a \tilde{U}^\dagger, \tag{28}$$

for an ensemble of size $N-N_0$, where $\tilde{P} = \tilde{U}\tilde{\Lambda}\tilde{U}^\dagger$. For each POVM element, we need to repeat the above procedure.

Furthermore, to guarantee that the infidelity scaling is improved to $O(1/N)$, one needs to carefully choose the probe states. Before showcasing how to do this, we first introduce several basic definitions. For a d-dimensional Hermitian space, we define bases $\mathscr{B}\left(\left\{|i\rangle_{i=1}^d\right\}\right)$ consisting of the following elements,

$$\sigma_i^z = |i\rangle\langle i| \quad (1 \le i \le d), \tag{29}$$

$$\sigma_{ij}^x = (|i\rangle\langle j| + |j\rangle\langle i|)/\sqrt{2} \quad (1 \le i < j \le d), \tag{30}$$

$$\sigma_{ij}^y = (-\mathrm{i}|i\rangle\langle j| + \mathrm{i}|j\rangle\langle i|)/\sqrt{2} \quad (1 \le i < j \le d), \tag{31}$$

where the set $\left\{|i\rangle_{i=1}^d\right\}$ is an arbitrary orthogonal basis. Note that all the operators are orthogonal w.r.t. the inner product $\langle A, B\rangle = \mathrm{Tr}\left(A^\dagger B\right)$. For a given basis $\{\xi_k\}_{k=1}^{K_1}$, denote span $\left\{\{\xi_k\}_{k=1}^{K_1}\right\}$ as the set of all finite real linear combinations of ξ_k $(1 \le k \le K_1)$. If span $\left\{\{\xi_k\}_{k=1}^{K_1}\right\}$ = span $\left\{\{\mu_k\}_{k=1}^{K_2}\right\}$, we say $\{\xi_k\}_{k=1}^{K_1}$ and $\{\mu_k\}_{k=1}^{K_2}$ are equivalent. If the span of the probe state set contains all d-dimensional Hermitian matrices and $M = d^2$, we say the probe state set is complete. If we further have $M > d^2$, we say it is over-complete.

In this section, we assume the true value of a rank r POVM element is P, the Step 1 estimation is $\tilde{P}$ and the Step 2 estimation is $\hat{P}$. The spectral decomposition of P is $P = \sum_{i=1}^d \lambda_i |\lambda_i\rangle\langle\lambda_i|$ where $\lambda_1 \ge \lambda_2 \ge \cdots \ge \lambda_r > 0$, $\lambda_{r+1} = \cdots = \lambda_d = 0$. In (29)–(31), if we change $\{|i\rangle\}$ to $\{|\lambda_i\rangle\}$ for $i = 1, \ldots, d$, we call this new basis $\mathscr{B}\left(\left\{|\lambda_i\rangle_{i=1}^d\right\}\right)$ *ideal bases*. If we change $\{|i\rangle\}$ to $\{|\lambda_i\rangle\}$ with i restricted in $[r+1, d]$, we call the set $\mathscr{B}\left(\left\{|\lambda_i\rangle_{i=r+1}^d\right\}\right)$ of these new $(d-r)^2$ elements as the *null bases* of P. If we change $\{|i\rangle\}$ to $\{|\lambda_i\rangle\}$ with i restricted in $[1, r]$, we call the set $\mathscr{B}\left(\left\{|\lambda_i\rangle_{i=1}^r\right\}\right)$ of these new r^2 elements as the *range bases* of P. After Step 1, we obtain an estimate $\tilde{P}$ and the spectral decomposition is $\tilde{P} = \sum_{i=1}^d \tilde{\lambda}_i \left|\tilde{\lambda}_i\right\rangle\left\langle\tilde{\lambda}_i\right|$. If we change $\{|i\rangle\}$ to $\{|\tilde{\lambda}_i\rangle\}$ for $i = 1, \ldots, d$, we call this new basis $\mathscr{B}\left(\left\{|\tilde{\lambda}_i\rangle_{i=1}^d\right\}\right)$ *estimated bases*. If we change $\{|i\rangle\}$ to $\{|\tilde{\lambda}_i\rangle\}$ with i restricted in $[r+1, d]$, we call the set $\mathscr{B}\left(\left\{|\tilde{\lambda}_i\rangle_{i=r+1}^d\right\}\right)$ of these new $(d-r)^2$ elements *estimated null bases*.

Then we give the following theorem as a guideline to design the probe state set.

Theorem 4. *For two-step adaptive QDT using arbitrary reconstruction algorithm with an $O(1/N)$ scaling for the MSE, suppose the resource number is N_0 in Step 1 and $N-N_0$ in Step 2, both evenly distributed for each probe state. The infidelity $\mathbb{E}\left(1 - F(\hat{P}, P)\right)$ of any rank-deficient POVM element scales as $O\left(\frac{1}{\sqrt{N_0(N-N_0)}}\right) + O\left(\frac{1}{N-N_0}\right)$ if*

- *(c1) the probe states in Step 1 are complete or over-complete;*
- *(c2) the probe states in Step 2 are complete or over-complete;*
- *(c3) the probe state set in Step 2 includes a subset equivalent to the $(d-r)^2$ estimated null basis $\mathscr{B}\left(\left\{|\tilde{\lambda}_i\rangle_{i=r+1}^d\right\}\right)$ from Step 1.*

We have the following corollary if we use GPB (generalized Pauli basis) states in Step 2.

Corollary 1. *For a POVM element P, using GPB states in Step 2, the infidelity reaches the optimal scaling $O(1/N)$ if $N_0 = \alpha N$ for certain $0 < \alpha < 1$.*

The proof is straightforward. If the POVM element P is full rank, it does not have first-order term and the infidelity scales as $O(1/N)$. If P is rank deficient with an unknown rank r, GPB states always satisfy Conditions (c1)–(c3) and thus the infidelity still scales as $O(1/N)$ by choosing $N_0 = \alpha N$ for certain $0 < \alpha < 1$. Because GPB states are effective for all cases, we will show their performance in Numerical Examples (Section 5).

We may use three methods to further make the estimation from Step 1 more accurate if the rank is not precise. The first one is to use Corollary 1. We use d^2 GPB states which always span the null basis. The second one is the possible scenario where we know the rank value from prior information. The third method is, from the rough estimation of Step 1, we may know an exact rank interval of the to-be-estimated POVM element. Since we know the upper bound of the estimated error as (9) here, we thus know the variation range of all the eigenvalues. Assume the rank interval is $[a, b]$ where $1 \le a < b \le d$, and $r \in [a, b]$ is the unknown rank. The more accurate is the estimation result from Step 1, the smaller is the interval length $b - a$. Then to ensure the infidelity scaling is $O(1/N)$, a conservative method is to add $(d-a)^2$ quantum states spanning the estimated null basis $\mathscr{B}\left(\left\{|\tilde{\lambda}_i\rangle_{i=a+1}^d\right\}\right)$.

Remark 6. The key in proving Theorem 4 is to characterize the first-order term, which is unaffected by the added term $-\left[\mathrm{Tr}\left(P_i - \hat{P}_i\right)\right]^2/d^2$ comparing (25) with (24). Hence, when (24) holds without distortion (see Proposition 3), one can still use (24) as the definition of fidelity, and GPB states still reach $O(1/N)$ scaling for the infidelity.

The choice of N_0 plays a key role in the performance of the two-step adaptive QDT. In this paper, we choose $N_0 = \frac{N}{2}$ and the infidelity scales as $O(1/N)$. Note that the infidelity behavior for different detector matrices can be different, even for binary detectors. For example, if $P_1 = U_1 \,\mathrm{diag}\,(1, 0, 0, 0)\, U_1^\dagger$ for certain unitary U_1 and $P_2 = I - P_1$, P_2's eigenvalues are 1, 1, 1, 0. Since P_2 has one zero eigenvalue, the infidelity reaches $O(1/\sqrt{N})$ by non-adaptive QDT. However, if $P_1 = U_1 \,\mathrm{diag}\,(0.1, 0, 0, 0)\, U_1^\dagger$, P_2's eigenvalues are 1, 1, 1, 0.9. Since P_2 has no zero eigenvalues, the infidelity can reach $O(1/N)$ by non-adaptive QDT. Therefore, for a complete characterization and analysis, we need to calculate the infidelity for every POVM element.

5. Numerical examples

Both the non-adaptive and adaptive QDT protocols need to prepare certain (in this paper pure) states $\{|\psi\rangle\}$ (we call them *ideal* states) as the probe states, which can be difficult to achieve in practice. As stated in Section 3.4, a realistic way in quantum optics experiments is to use the superposition of coherent states to approximate the ideal states. In this section we demonstrate the performance of our optimal and adaptive protocols both using ideal probe states and using superposed coherent probe states. We use the two-stage QDT reconstruction algorithm for numerical simulations.

5.1. Optimal detector tomography

For non-adaptive QDT in $d = 4$ systems, we test 14 different protocols using different probe states in Table 1. In protocols 1–5, we compare $M\,\mathrm{Tr}\left[(X^TX)^{-1}\right]$ and condition numbers of ideal pure states such as MUB, Cube, SIC, GPB probe states which are

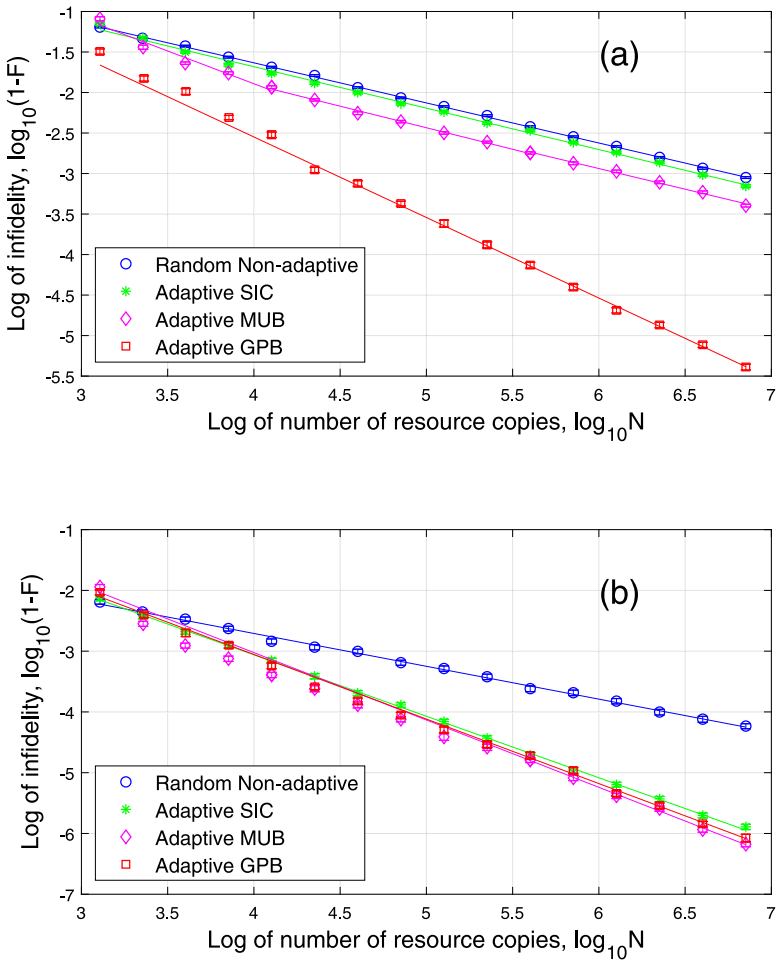

Fig. 2. Infidelity for binary detectors with given unitary matrix U_1 in (33). (a) P_1; (b) P_2.

Table 1
Comparison of various four-dimensional QDT protocols.

Protocol	Probe states	Number(M)	$M\,\mathrm{Tr}\left[(X^TX)^{-1}\right]$	cond(X)
1	SIC	16	304[a]	$\sqrt{5}$[a]
2	MUB	20	304[a]	$\sqrt{5}$[a]
3	Cube[b]	36	400	3
4	GPB	16	640	$\sqrt{\frac{9+\sqrt{73}}{9-\sqrt{73}}}$
5	Random pure	32	629.16	2.39
6	1-coherent SIC	16	2.48×10^4	307.11
7	1-coherent MUB	20	2.46×10^3	82.37
8	1-coherent Random	32	9.81×10^3	26.03
9	2-coherent SIC	16	400.61	3.44
10	2-coherent MUB	20	470.67	3.27
11	2-coherent Random	32	607.35	5.48
12	3-coherent SIC	16	352.82	2.79
13	3-coherent MUB	20	364.01	2.60
14	3-coherent Random	32	532.85	4.95

[a]This is the optimal value.
[b]Cube states are product probe states.

constructed as Appendix A in Xiao, Wang et al. (2021). "Cube" states here are product states of one-qubit MUB states, assuming that the $d = 4$ system here is the composition of two $d = 2$ systems. GPB states are similar to the optimal measurement-generalized Pauli operators in Miranowicz et al. (2014). "Random Pure" means that we generate 32 random pure states using the algorithm in Miszczak (2012) and Zyczkowski and Kus (1994) where $M\,\mathrm{Tr}\left[(X^TX)^{-1}\right]$ and condition number are obtained by the average of 1000 results. We find SIC states and MUB states have the minimum value of $M\,\mathrm{Tr}\left[(X^TX)^{-1}\right]$ as 304 and minimum condition number as $\sqrt{5}$, satisfying Theorem 1. For two-qubit product states—Cube states which are easier to generate in experiment, the values of UMSE and condition number are 400 and 3, respectively, a little larger than the optimal values and satisfying Theorem 2.

In protocols 6–14, we use superposition of n_c ($n_c = 1, 2, 3$) coherent states (denoted as n_c-coherent SIC/MUB) to approximate the four-dimensional SIC and MUB states by solving the optimization problem (19). The case of $n_c = 1$ is using one coherent state without superposition. As a comparison, we also add the protocols of using the superposition of n_c random coherent states (denoted as n_c-coherent Random). The random algorithm is the same as the coherent states preparation procedure in Wang et al. (2021). The optimization landscape might have local minima. Therefore, we run the optimization algorithm with 100 different initial values and choose the best result.

We find for one coherent state, it cannot approximate SIC and MUB states well and both the condition number and UMSE are large. For the superposition of two and three coherent states, they can approximate SIC and MUB states well and the corresponding condition number and UMSE are close to the optimal values, and smaller than 2,3-coherent Random protocols. Also, with n_c increasing, the superposition result becomes close to ideal probe states and thus the UMSE and condition number decrease.

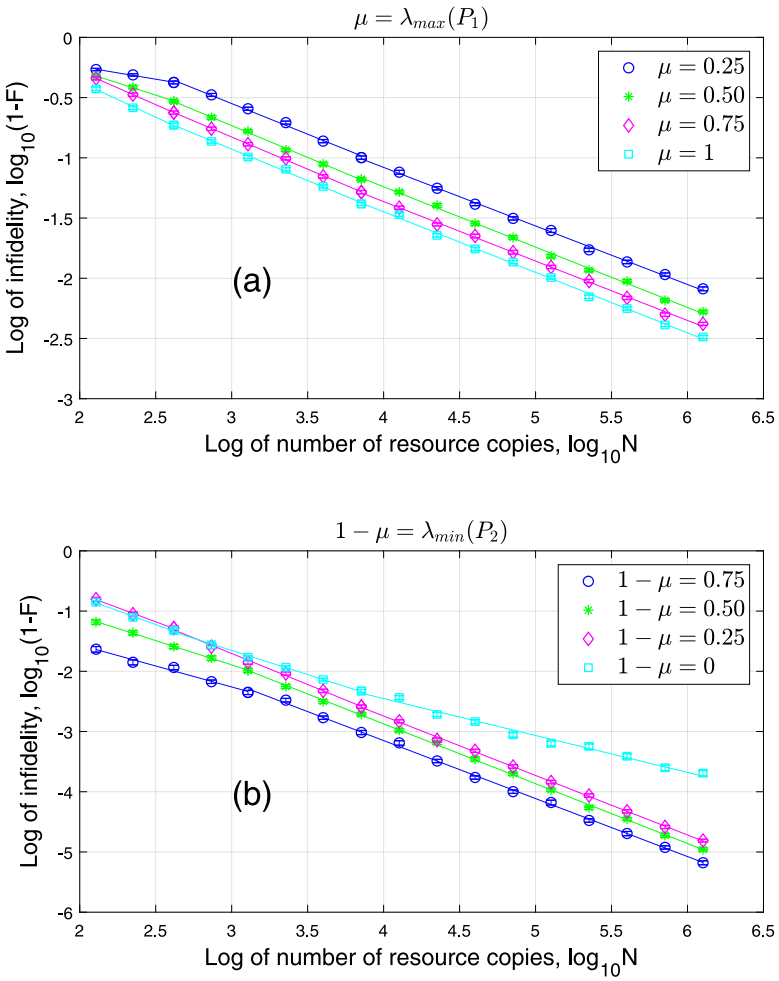

Fig. 3. Infidelity for non-adaptive tomography with different eigenvalues μ of binary detectors. (a) P_1; (b) P_2.

5.2. Adaptive QDT using ideal probe states

5.2.1. Binary detectors

For binary detectors $P_1 + P_2 = I$, P_1 and P_2 can be simultaneously diagonalized by a common unitary (Wang et al., 2019). Hence, the eigenvalues of P_1 will affect the eigenvalues of P_2. This determines the rank of P_2, which will further influence the scaling of non-adaptive tomography. Let

$$P_1 = U_1 \,\mathrm{diag}\,(\mu, 0, 0, 0)\, U_1^\dagger. \tag{32}$$

With non-adaptive tomography, when $\mu < 1$, P_2 is full-ranked and the infidelity of estimating P_2 scales as $O(1/N)$, while for $\mu = 1$, P_2 is rank-deficient and the infidelity of estimating P_2 scales as $O(1/\sqrt{N})$.

Therefore, we firstly consider a binary detector for $\mu = 1$ where

$$P_1 = U_1 \,\mathrm{diag}\,(1, 0, 0, 0)\, U_1^\dagger. \tag{33}$$

This detector is fully specified by the projection measurement P_1. The matrix U_1 is randomly generated using the algorithm in Johnston (2016) and Zyczkowski and Kus (1994). For each resource number, we run the algorithm 100 times and obtain the average infidelity and standard deviation.

The four curves in Fig. 2 are as follows:

- Random Non-adaptive: We only have Step 1 and choose 48 random pure states.
- Adaptive SIC: In Step 1, we use 16 SIC states $\left\{\rho_j^{(\mathrm{SIC})}\right\}$ and in Step 2, we use 32 new states as (28).
- Adaptive MUB: In Step 1, we use 20 MUB states $\left\{\rho_j^{(\mathrm{MUB})}\right\}$ and in Step 2, we use 40 new states as (28).
- Adaptive GPB: In Step 1, we use 16 GPB states and in Step 2, we use 32 new GBP states by replacing the set $\{|i\rangle\}$ by $\left\{\left|\tilde{\lambda}_i\right\rangle\right\}$ as shown in Appendix A in Xiao, Wang et al. (2021).

As shown in Fig. 2, Random Non-adaptive tomography only reaches $1 - F = O(1/\sqrt{N})$ for both P_1 and P_2 because they both have zero eigenvalues and the first-order term scales as $O(1/\sqrt{N})$. Adaptive GPB tomography can reach $1-F = O(1/N)$ for P_1 and P_2 as proved in Corollary 1. For adaptive SIC and MUB tomography, they can only reach $1 - F = O(1/\sqrt{N})$ for P_1 probably because adaptive SIC and MUB states do not have a subset equivalent to the 9 estimated null bases and do not satisfy Condition (c3) in Theorem 4. They can reach $1-F = O(1/N)$ for P_2 because adaptive SIC and MUB states have a subset equivalent to the estimated null basis and satisfy Condition (c3).

Then we show infidelity for non-adaptive tomography with different eigenvalues $\mu = 0.25, 0.5, 0.75, 1$ in (32) of binary detectors in Fig. 3. For each resource number, we run the algorithm 100 times and obtain the average infidelity and the standard deviation. Because P_1 is always rank deficient, the infidelity for P_1 scales as $O(1/\sqrt{N})$. As μ increases, the measurement accuracy increases and thus the infidelity of P_1 becomes smaller for a given N. Because P_2 is full rank for $\mu < 1$, its infidelity scales as $O(1/N)$. In addition, the infidelity of P_2 becomes larger as μ increases for

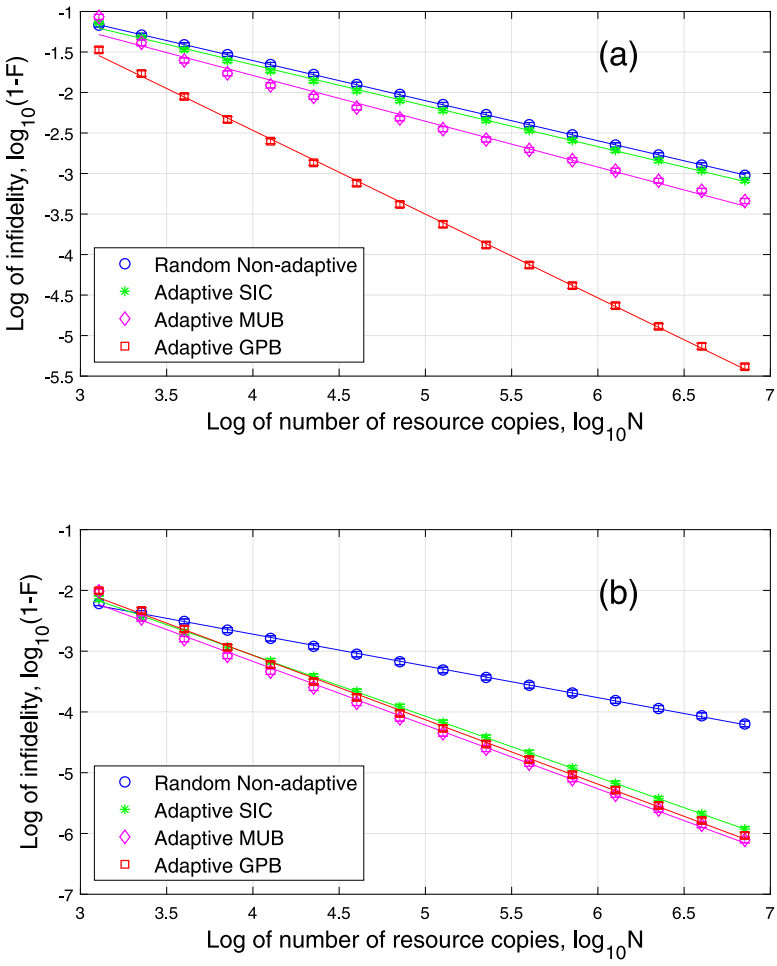

Fig. 4. Infidelity for 200 different binary detectors by changing U_1 in (33). (a) P_1; (b) P_2.

a given N. When μ increases to 1, both the infidelities of P_1 and P_2 scale as $O(1/\sqrt{N})$ because they are both rank deficient.

To test the robustness of our adaptive protocol, we perform adaptive QDT on 200 random binary detectors in the form of (33) by changing the unitary matrix U_1 which is randomly created using the algorithm in Johnston (2016) and Zyczkowski and Kus (1994). For each U_1, we run our tomography algorithm 100 times and obtain the mean infidelities for given resource number N. Then we calculate the mean values and the standard deviations of these 200 mean infidelities. The result is shown in Fig. 4. It is clear that Adaptive GPB tomography can reach $1 - F = O(1/N)$ for P_1 and P_2. In addition, all the standard deviations are small, which demonstrates that our Adaptive GPB protocol is robust.

We then consider the case that P_1 is a perturbed projection measurement,

$$\begin{aligned} &P_1 + P_2 = I, \\ &P_1 = U_1 \,\mathrm{diag}\,(0.6, 0.001, 0.001, 0.001)\, U_1^\dagger. \end{aligned} \tag{34}$$

The tomography errors are shown in Fig. 5. From Fig. 5(a), we can see that the curves of adaptive QDT can be roughly divided into three segments from left to right for the detector P_1, which is similar to the phenomenon in QST (Qi et al., 2017). In the first segment, the resource number is not large enough ($N \leq 10^4$) and the near-zero eigenvalues are not strong enough to make a difference from zero. The performance is thus the same as projection measurement. Hence, the infidelity decreases as $O(1/N)$ firstly. When the resource number increases ($10^4 \leq N \leq 10^{5.5}$), the near-zero eigenvalues start to take effect. We cannot distinguish them from zero accurately and thus the infidelity scales as $O(1/\sqrt{N})$. Finally, when the resource number is large enough ($N \geq 10^{5.5}$) to clearly distinguish between the near-zero eigenvalues and zero, we are performing full rank detector tomography actually, which has $O(1/N)$ decay rate for infidelity. For Random Non-adaptive tomography, it can be divided into two segments. When the resource number is not enough ($N \leq 10^{6.5}$) to estimate the near-zero eigenvalues accurately, the infidelity decreases as $O(1/\sqrt{N})$. When the resource number is large enough ($N \geq 10^{6.5}$) to clearly distinguish between the near-zero eigenvalues and zero, the infidelity scales as $O(1/N)$. Overall, the Adaptive GPB tomography is the best among these methods.

For detector P_2, all the eigenvalues are significantly larger than zero, and P_2 is full-rank. Hence, the infidelity decreases as $O(1/N)$ for both non-adaptive and adaptive tomography.

5.2.2. Three-valued detectors

Three-valued detectors are different from binary detectors because three-valued detector matrices generally cannot be diagonalized by the same unitary matrix like binary detectors. We consider a three-valued detector as

$$\begin{aligned} &P_1 + P_2 + P_3 = I, \\ &P_1 = U_1 \,\mathrm{diag}\,(0.4, 0, 0, 0)\, U_1^\dagger = 0.4 U_1 (|00\rangle\langle 00|) U_1^\dagger, \\ &P_2 = U_2 \,\mathrm{diag}\,(0, 0.5, 0, 0)\, U_2^\dagger = 0.5 U_2 (|01\rangle\langle 01|) U_2^\dagger. \end{aligned} \tag{35}$$

This detector is constructed from two-qubit MUB measurement (see Appendix A in Xiao, Wang et al. (2021)). The first detector P_1 is from $|00\rangle$ where we product a coefficient 0.4 and conjugate

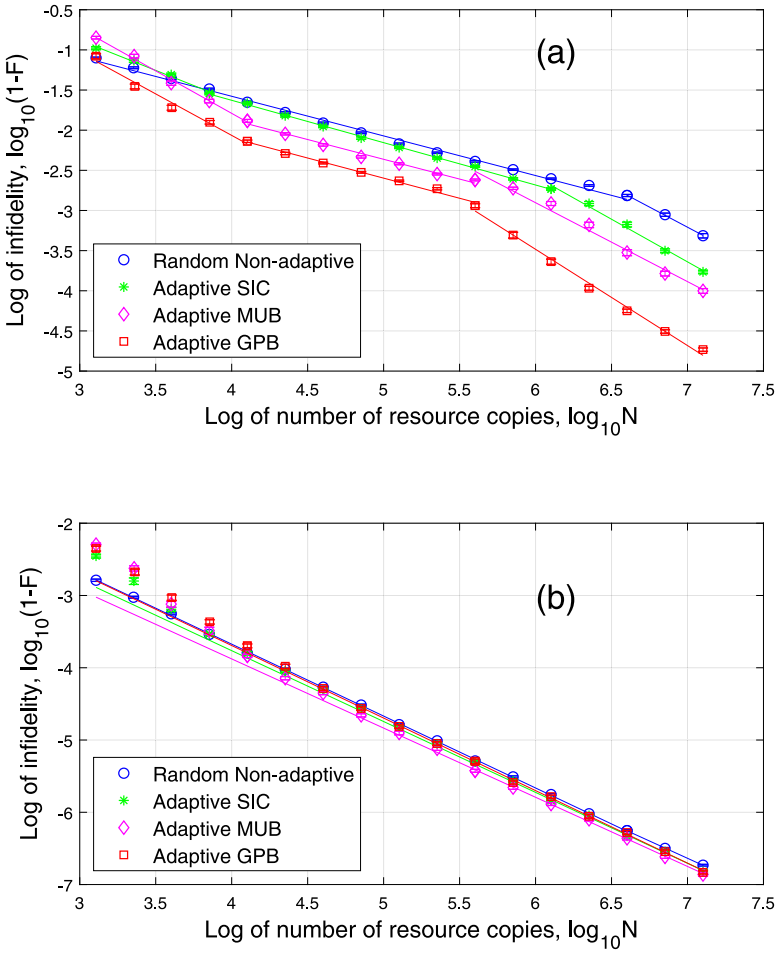

Fig. 5. Infidelity for binary detectors in (34). (a) P_1; (b) P_2.

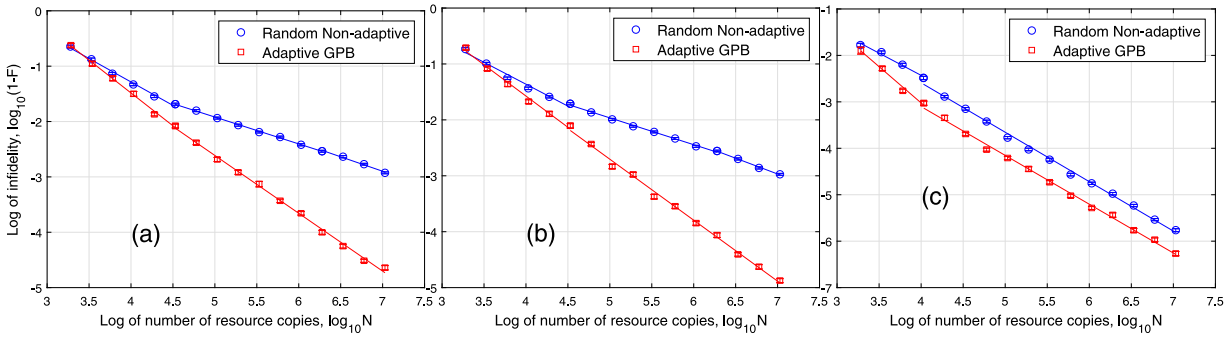

Fig. 6. Infidelity for three-valued detectors with given unitary matrices U_1 and U_2 in (35). (a) P_1; (b) P_2; (c) P_3.

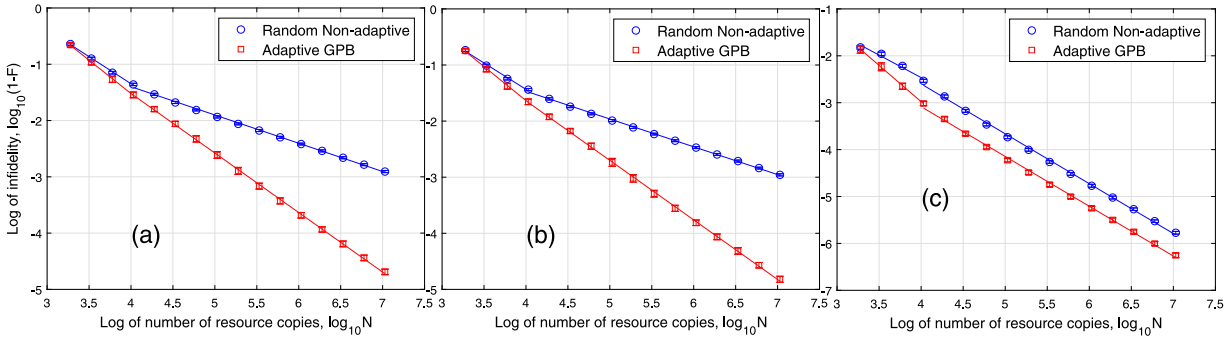

Fig. 7. Infidelity for 200 different three-valued detectors by changing U_1 and U_2 in (35). (a) P_1; (b) P_2; (c) P_3.

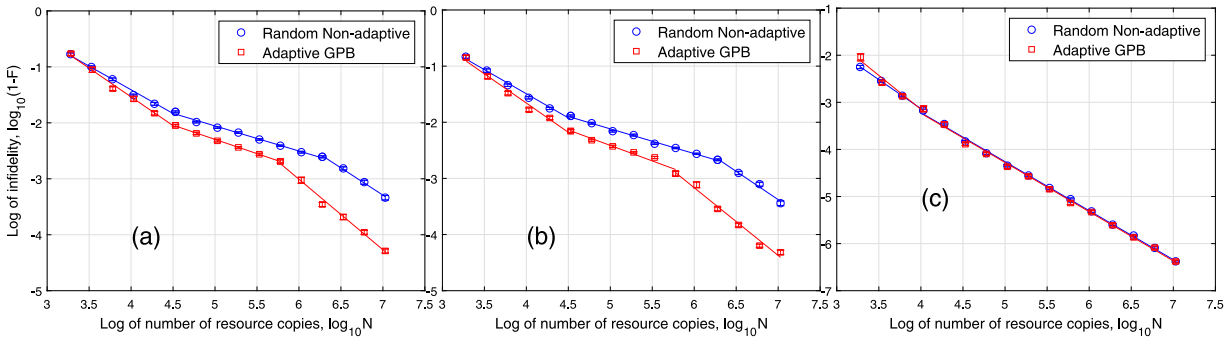

Fig. 8. Infidelity for three-valued detectors in (36). (a) P_1; (b) P_2; (c) P_3.

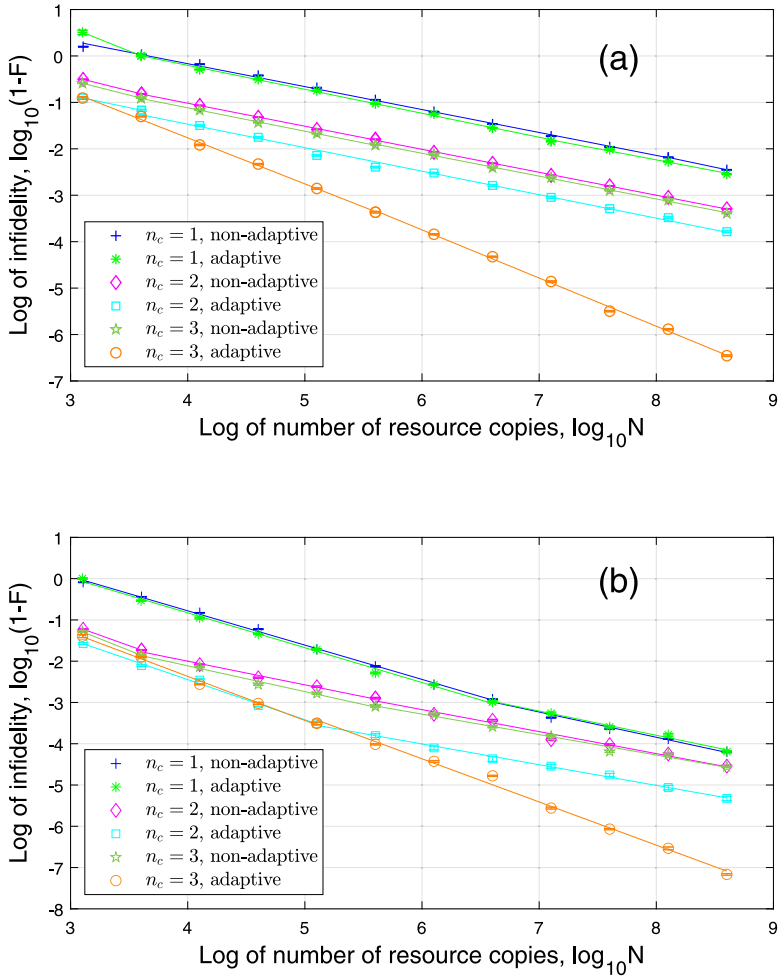

Fig. 9. Superposition of n_c-coherent states for (33) where $n_c = 1, 2, 3$. (a) P_1; (b) P_2.

a unitary rotation U_1. In a similar way, P_2 is from $|01\rangle$ where we product a coefficient 0.5 and conjugate a unitary rotation U_2. We can prove that $P_3 = I - P_1 - P_2$ is always positive semidefinite. The unitary rotations U_1 and U_2 are generated by the random unitary algorithm in Johnston (2016) and Zyczkowski and Kus (1994). For each resource number, we run the algorithm 100 times and obtain the average infidelity and standard deviation. We focus on the comparison between Adaptive GPB tomography and Random Non-adaptive tomography. The simulation result is in Fig. 6 where our adaptive tomography can reach $O(1/N)$ for P_1 and P_2 as proved in Corollary 1, improving the $O(1/\sqrt{N})$ scaling of non-adaptive tomography. For P_3, all the eigenvalues are far from zero and both tomography methods can reach $O(1/N)$. We also test robustness by performing adaptive QDT on 200 random three-valued detectors in the form of (35) by changing unitary matrices U_1 and U_2, which is similar as binary detectors. The result is shown in Fig. 7. For P_1 and P_2, the adaptive tomography is robust (with small standard deviation) and their infidelities can reach $O(1/N)$. For full rank P_3, both tomography methods can reach $O(1/N)$. Then we consider that P_1 and P_2 have three small eigenvalues as

$$\begin{aligned} &P_1 + P_2 + P_3 = I, \\ &P_1 = U_1 \,\mathrm{diag}\,(0.4, 0.001, 0.001, 0.001)\, U_1^\dagger, \\ &P_2 = U_2 \,\mathrm{diag}\,(0.001, 0.5, 0.001, 0.001)\, U_2^\dagger. \end{aligned} \tag{36}$$

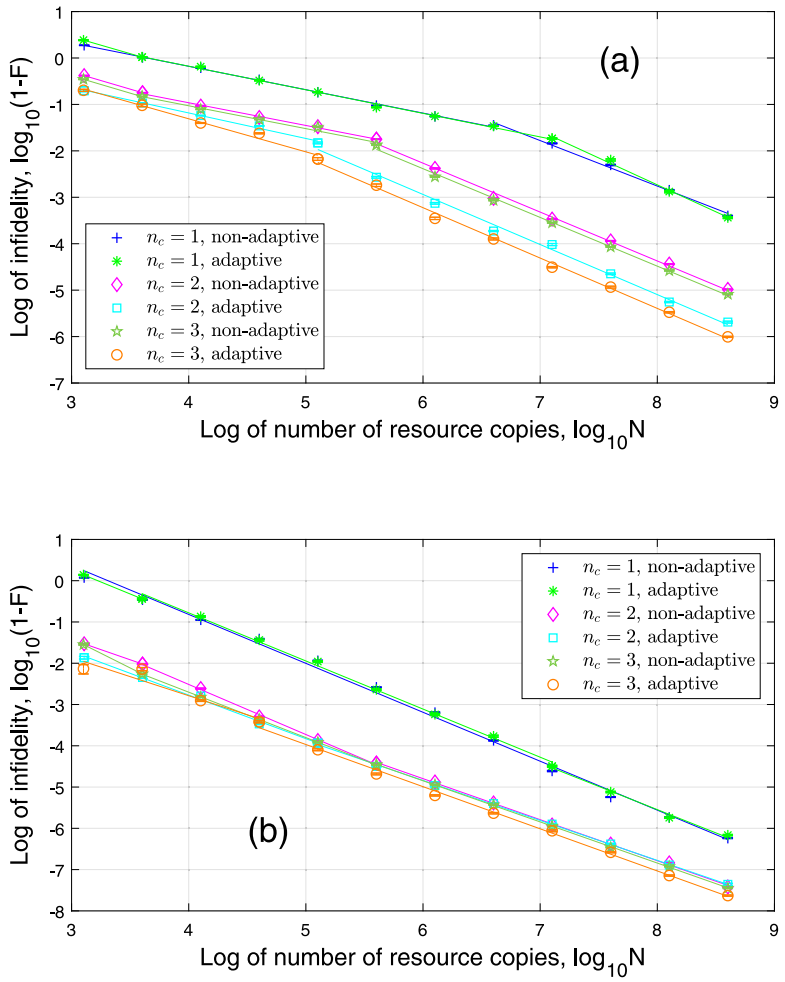

Fig. 10. Superposition of n_c-coherent states for (34) where $n_c = 1, 2, 3$. (a) P_1; (b) P_2.

The results for P_1 and P_2 can also be divided into three segments as shown in Fig. 8 and we have explained for binary detectors. For P_3, all the eigenvalues are far from zero and hence, both tomography can reach $O(1/N)$.

5.3. Adaptive QDT using coherent states

Since the adaptive GPB states can improve the infidelity for all detectors if they have zero or near-zero eigenvalues, in this part, we use the superposition of coherent states to approximate the ideal adaptive GPB states. We consider binary detectors as (33). We use n_c-coherent states as shown in Fig. 9 where $n_c = 1, 2, 3$. For given n_c, the adaptive tomography performance is usually better than non-adaptive one. As n_c increases, the approximation error decreases. When the resource number N is not large enough to distinguish the approximation error, the infidelity scales close to $O(1/N)$, like $n_c = 2$, adaptive for P_2 in Fig. 9(b) when $N \leq 10^5$. When $N \geq 10^5$, the infidelity scales to $O(1/\sqrt{N})$ because of the approximation error.

For binary detectors as (34), the similar results are shown in Fig. 10. For P_1, all the curves can be roughly divided into two segments. For 1-coherent state, the infidelity scales as $O(1/\sqrt{N})$ when $N \leq 10^7$ and scales as $O(1/N)$ when $N \geq 10^7$. For 2,3-coherent states, the infidelity scales as $O(1/\sqrt{N})$ when $N \leq 10^6$ and scales as $O(1/N)$ when $N \geq 10^6$. This result is similar to Fig. 5 without the first segment. For P_2, the infidelity scales as $O(1/N)$ because all the eigenvalues are significantly larger than zero.

6. Conclusion

In this paper we have investigated how to optimize the probe states in quantum detector tomography. We have characterized the optimal probe state sets based on minimizing the UMSE and minimizing the condition number. We have proven that SIC and MUB states are optimal. In the adaptive scenario we have proposed a two-step strategy to adaptively optimize the probe states, and proven that our strategy can improve the modified infidelity from $O(1/\sqrt{N})$ to $O(1/N)$ under certain conditions. Numerical examples were presented to demonstrate the effectiveness of our strategies.

Acknowledgments

Y. Wang would like to thank Prof. Howard M. Wiseman for the helpful discussion. We thank the anonymous referees and the Associate Editor for their constructive comments.

References

Adamson, R. B. A., & Steinberg, A. M. (2010). Improving quantum state estimation with mutually unbiased bases. *Physical Review Letters*, *105*, Article 030406.

Boyd, S., & Vandenberghe, L. (2004). *Convex optimization*. Cambridge University Press.

Brida, G., Ciavarella, L., Degiovanni, I. P., Genovese, M., Lolli, L., Mingolla, M. G., et al. (2012). Quantum characterization of superconducting photon counters. *New Journal of Physics*, *14*(8), Article 085001.

Brida, G., Ciavarella, L., Degiovanni, I. P., Genovese, M., Migdall, A., Mingolla, M. G., et al. (2012). Ancilla-assisted calibration of a measuring apparatus. *Physical Review Letters*, *108*, Article 253601.

Degen, C. L., Reinhard, F., & Cappellaro, P. (2017). Quantum sensing. *Reviews of Modern Physics*, *89*, Article 035002.

DiVincenzo, D. P. (1995). Quantum computation. *Science*, *270*(5234), 255–261.

Durt, T., Englert, B.-G., Bengtsson, I., & Życzkowski, K. (2010). On mutually unbiased bases. *International Journal of Quantum Information*, *08*(04), 535–640.

Feito, A., Lundeen, J. S., Coldenstrodt-Ronge, H., Eisert, J., Plenio, M. B., & Walmsley, I. A. (2009). Measuring measurement: theory and practice. *New Journal of Physics*, *11*(9), Article 093038.

Fiurášek, J. (2001). Maximum-likelihood estimation of quantum measurement. *Physical Review A*, *64*, Article 024102.

Fiurášek, J., & Hradil, Z. (2001). Maximum-likelihood estimation of quantum processes. *Physical Review A*, *63*, Article 020101.

Grandi, S., Zavatta, A., Bellini, M., & Paris, M. G. A. (2017). Experimental quantum tomography of a homodyne detector. *New Journal of Physics*, *19*(5), Article 053015.

Hou, Z., Zhong, H. S., Tian, Y., Dong, D., Qi, B., Li, L., et al. (2016). Full reconstruction of a 14-qubit state within four hours. *New Journal of Physics*, *18*(8), Article 083036.

Hübner, M. (1992). Explicit computation of the bures distance for density matrices. *Physics Letters A*, *163*(4), 239–242.

Huszár, F., & Houlsby, N. M. T. (2012). Adaptive Bayesian quantum tomography. *Physical Review A*, *85*, Article 052120.

Janszky, J., Domokos, P., Szabó, S., & Adam, P. (1995). Quantum-state engineering via discrete coherent-state superpositions. *Physical Review A*, *51*, 4191–4193.

Johnston, N. (2016). QETLAB: A MATLAB toolbox for quantum entanglement, version 0.9.

Jozsa, R. (1994). Fidelity for mixed quantum states. *Journal of Modern Optics*, *41*(12), 2315–2323.

Kravtsov, K. S., Straupe, S. S., Radchenko, I. V., Houlsby, N. M. T., Huszár, F., & Kulik, S. P. (2013). Experimental adaptive Bayesian tomography. *Physical Review A*, *87*, Article 062122.

Lundeen, J. S., Feito, A., Coldenstrodt-Ronge, H., Pregnell, K. L., Silberhorn, C., Ralph, T. C., et al. (2009). Tomography of quantum detectors. *Nature Physics*, *5*(1), 27–30.

Mahler, D. H., Rozema, L. A., Darabi, A., Ferrie, C., Blume-Kohout, R., & Steinberg, A. M. (2013). Adaptive quantum state tomography improves accuracy quadratically. *Physical Review Letters*, *111*, Article 183601.

Miranowicz, A., Bartkiewicz, K., Peřina, J., Koashi, M., Imoto, N., & Nori, F. (2014). Optimal two-qubit tomography based on local and global measurements: Maximal robustness against errors as described by condition numbers. *Physical Review A*, *90*, Article 062123.

Miszczak, J. A. (2012). Generating and using truly random quantum states in mathematica. *Computer Physics Communications*, *183*(1), 118–124.

Mu, B., Qi, H., Petersen, I. R., & Shi, G. (2020). Quantum tomography by regularized linear regressions. *Automatica*, *114*, Article 108837.

Natarajan, C. M., Zhang, L., Coldenstrodt-Ronge, H., Donati, G., Dorenbos, S. N., Zwiller, V., et al. (2013). Quantum detector tomography of a time-multiplexed superconducting nanowire single-photon detector at telecom wavelengths. *Optics Express*, *21*(1), 893–902.

Nielsen, M. A., & Chuang, I. L. (2010). *Quantum computation and quantum information*. Cambridge University Press.

Pereira, L., Zambrano, L., Cortés-Vega, J., Niklitschek, S., & Delgado, A. (2018). Adaptive quantum tomography in high dimensions. *Physical Review A*, *98*, Article 012339.

Qi, B., Hou, Z., Li, L., Dong, D., Xiang, G.-Y., & Guo, G.-C. (2013). Quantum state tomography via linear regression estimation. *Scientific Reports*, *3*, Article 3496.

Qi, B., Hou, Z., Wang, Y., Dong, D., Zhong, H.-S., Li, L., et al. (2017). Adaptive quantum state tomography via linear regression estimation: Theory and two-qubit experiment. *npj Quantum Information*, *3*, Article 19.

Renema, J. J., Frucci, G., Zhou, Z., Mattioli, F., Gaggero, A., Leoni, R., et al. (2012). Modified detector tomography technique applied to a superconducting multiphoton nanodetector. *Optics Express*, *20*(3), 2806–2813.

Renes, J. M., Blume-Kohout, R., Scott, A. J., & Caves, C. M. (2004). Symmetric informationally complete quantum measurements. *Journal of Mathematical Physics*, *45*(6), 2171–2180.

Scott, A. J. (2017). SICs: Extending the list of solutions. Quant-Ph, arXiv:1703.03993.

Sone, A., & Cappellaro, P. (2017a). Exact dimension estimation of interacting qubit systems assisted by a single quantum probe. *Physical Review A*, *96*, Article 062334.

Sone, A., & Cappellaro, P. (2017b). Hamiltonian identifiability assisted by a single-probe measurement. *Physical Review A*, *95*, Article 022335.

Struchalin, G. I., Pogorelov, I. A., Straupe, S. S., Kravtsov, K. S., Radchenko, I. V., & Kulik, S. P. (2016). Experimental adaptive quantum tomography of two-qubit states. *Physical Review A*, *93*, Article 012103.

Szabo, S., Adam, P., Janszky, J., & Domokos, P. (1996). Construction of quantum states of the radiation field by discrete coherent-state superpositions. *Physical Review A*, *53*, 2698–2710.

Wang, Y., Dong, D., Qi, B., Zhang, J., Petersen, I. R., & Yonezawa, H. (2018). A quantum Hamiltonian identification algorithm: Computational complexity and error analysis. *IEEE Transactions on Automatic Control*, *63*(5), 1388–1403.

Wang, Y., Dong, D., Sone, A., Petersen, I. R., Yonezawa, H., & Cappellaro, P. (2020). Quantum Hamiltonian identifiability via a similarity transformation approach and beyond. *IEEE Transactions on Automatic Control*, *65*(11), 4632–4647.

Wang, Y., Dong, D., & Yonezawa, H. (2019). Tomography of binary quantum detectors. In *Proc. of 2019 IEEE 58th Conference on Decision and Control (CDC)* (pp. 396–400). http://dx.doi.org/10.1109/CDC40024.2019.9029759.

Wang, Y., Yin, Q., Dong, D., Qi, B., Petersen, I. R., Hou, Z., et al. (2019). Quantum gate identification: Error analysis, numerical results and optical experiment. *Automatica*, *101*, 269–279.

Wang, Y., Yokoyama, S., Dong, D., Petersen, I. R., Huntington, E. H., & Yonezawa, H. (2021). Two-stage estimation for quantum detector tomography: Error analysis, numerical and experimental results. *IEEE Transactions on Information Theory*, *67*(4), 2293–2307.

Wünsche, A., Dodonov, V., Man'ko, O., & Man'ko, V. (2001). Nonclassicality of states in quantum optics. *Fortschritte Der Physik*, *49*(10–11), 1117–1122.

Xiao, S., Wang, Y., Dong, D., & Zhang, J. (2021). Optimal and two-step adaptive quantum detector tomography. quant-ph, arXiv:2106.09255v2,

Xiao, S., Wang, Y., Dong, D., & Zhang, J. (2021). Optimal quantum detector tomography via linear regression estimation. In *Proc. of 2021 IEEE 60th Conference on Decision and Control (CDC)* (pp. 4140–4145). http://dx.doi.org/10.1109/CDC45484.2021.9683213.

Xiao, S., Xue, S., Dong, D., & Zhang, J. (2021). Identification of time-varying decoherence rates for open quantum systems. *IEEE Transactions on Quantum Engineering*, *2*, Article 2102212.

Yu, Q., Dong, D., Wang, Y., & Petersen, I. R. (2020). Adaptive quantum process tomography via linear regression estimation. In *Proc. of 2020 International Conference on Systems, Man, and Cybernetics (SMC)* (pp. 4173–4178). http://dx.doi.org/10.1109/SMC42975.2020.9283060.

Yu, Q., Wang, Y., Dong, D., & Petersen, I. R. (2021). On the capability of a class of quantum sensors. *Automatica*, *129*, Article 109612.

Zhang, L., Coldenstrodt-Ronge, H. B., Datta, A., Puentes, G., Lundeen, J. S., Jin, X.-M., et al. (2012). Mapping coherence in measurement via full quantum tomography of a hybrid optical detector. *Nature Photonics*, *6*(6), 364.

Zhang, L., Datta, A., Coldenstrodt-Ronge, H. B., Jin, X.-M., Eisert, J., Plenio, M. B., et al. (2012). Recursive quantum detector tomography. *New Journal of Physics*, *14*(11), Article 115005.

Zhang, J., & Sarovar, M. (2014). Quantum Hamiltonian identification from measurement time traces. *Physical Review Letters*, *113*, Article 080401.

Zhang, J., & Sarovar, M. (2015). Identification of open quantum systems from observable time traces. *Physical Review A*, *91*, Article 052121.

Zhang, A., Xie, J., Xu, H., Zheng, K., Zhang, H., Poon, Y.-T., et al. (2020). Experimental self-characterization of quantum measurements. *Physical Review Letters*, *124*, Article 040402.

Zhu, H. (2012). *Quantum state estimation and symmetric informationally complete POMs* (Ph.D. thesis), National University of Singapore.

Zyczkowski, K., & Kus, M. (1994). Random unitary matrices. *Journal of Physics A: Mathematical and General*, *27*(12), 4235–4245.

Shuixin Xiao received a B.E. degree in automation from Huazhong University of Science and Technology, Wuhan, China, in 2018. He is currently working toward the Ph.D. degree in a joint Ph.D. program with Shanghai Jiao Tong University, Shanghai, China, and the University of New South Wales, Canberra, ACT, Australia. His current research interests include quantum system identification, quantum computing and quantum information processing.

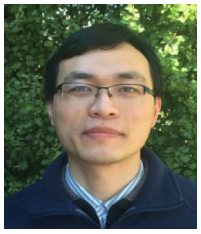

Yuanlong Wang received a B.E. degree in automation from Northeastern University, Shenyang, China, in 2011, an M.E. degree in control science and engineering from Zhejiang University, Hangzhou, China, in 2015, and a Ph.D. degree in engineering from the University of New South Wales, Canberra, ACT, Australia, in 2019. He was a Post-Doctoral Fellow with the Centre for Quantum Dynamics, Griffith University, Brisbane, QLD, Australia, from 2019 to 2022. He is now an Associate Professor in the Academy of Mathematics and Systems Science, Chinese Academy of Sciences, Beijing, China. His research interests include quantum control theory and quantum parameter estimation theory.

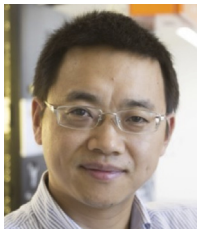

Daoyi Dong is currently a Scientia Associate Professor at the University of New South Wales, Canberra, Australia. He received a B.E. degree in automatic control and a Ph.D. degree in engineering from the University of Science and Technology of China, Hefei, China, in 2001 and 2006, respectively. He was with the Institute of Systems Science, Chinese Academy of Sciences and with Zhejiang University. He had visiting positions at Princeton University, NJ, USA, RIKEN, Wako-Shi, Japan, University of Duisburg–Essen, Germany and The University of Hong Kong, Hong Kong.

His research interests include quantum control and machine learning. Dr. Dong was awarded an ACA Temasek Young Educator Award by The Asian Control Association and is a recipient of an International Collaboration Award and an Australian Post-Doctoral Fellowship from the Australian Research Council, and a Humboldt Research Fellowship from the Alexander von Humboldt Foundation of Germany. He is a Member-at-Large, Board of Governors, and was the Associate Vice President for Conferences & Meetings, IEEE Systems, Man and Cybernetics Society. He served as an Associate Editor of IEEE Transactions on Neural Networks and Learning Systems (2015–2021). He is currently an Associate Editor of IEEE Transactions on Cybernetics, and a Technical Editor of IEEE/ASME Transactions on Mechatronics.

Jun Zhang received the B.S. degree in Automatic Control from Shanghai Jiao Tong University, China, in 1993, and the M.S. and Ph.D. degrees in Electrical Engineering from the University of California at Berkeley, CA, USA in 1999 and 2003, respectively. Later he worked as a research specialist at Berkeley Chemistry department, and also as a staff engineer at several high tech firms in the Silicon Valley. He is currently a Research Fellow at the Joint Institute of UMich-SJTU in Shanghai Jiao Tong University.

His current research interests include quantum control, process and motion control.